Influence of Polymer Backbone Fluorination on the Electrochemical Behavior of Single-Ion Conducting Multiblock Copolymer Electrolytes

Alexander Mayer, Huu-Dat Nguyen, Alessandro Mariani, Thomas Diemant, Sandrine Lyonnard, Cristina Iojoiu, Stefano Passerini, Dominic Bresser

Influence of Polymer Backbone Fluorination on the Electrochemical Behavior of Single-Ion Conducting Multi-Block Copolymer Electrolytes

Alexander Mayer[a,b], Huu-Dat Nguyen[c,#], Alessandro Mariani[a,b,†], Thomas Diemant[a,b], Cristina Iojoiu[c,d,*], Stefano Passerini[a,b,*], and Dominic Bresser[a,b,*]

a Helmholtz Institute Ulm (HIU), Helmholtzstrasse 11, 89081 Ulm, Germany

b Karlsruhe Institute of Technology (KIT), P.O. Box 3640, 76021 Karlsruhe, Germany

c Univ. Grenoble Alpes, Univ. Savoie Mont Blanc, CNRS, Grenoble INP, LEPMI, UMR5279, 38000 Grenoble, France

d Réseau sur le Stockage Electrochimique de l'Energie (RS2E), CNRS FR3459, 80039 Amiens, France

KEYWORDS: block copolymer, single-ion conductor, fluorination, lithium battery, polymer electrolyte

ABSTRACT: The presence of fluorine, especially in the electrolyte, frequently has a beneficial effect on the performance of lithium batteries owing to, for instance, the stabilization of the interfaces and interphases with the positive and negative electrode. However, the presence of fluorine is also associated with reduced recyclability and low biodegradability. Herein, we present a single-ion conducting multi-block copolymer electrolyte comprising a fluorine-free backbone and compare it with the fluorinated analogue reported earlier. Following a comprehensive physicochemical and electrochemical characterization of the copolymer with the fluorine-free backbone, the focus of the comparison with the fluorinated analogue was particularly on the electrochemical stability towards oxidation and reduction as well as the reactions occurring at the interface with the lithium-metal electrode. To deconvolute the impact of the fluorine in the ionic side chain and the copolymer backbone, suitable model compounds were identified and studied experimentally and theoretically. The results show that the absence of fluorine in the backbone has little impact on the basic electrochemical properties such as the ionic conductivity, but severely affects the electrochemical stability and interfacial stability. The results highlight the need for a very careful design of the whole polymer for each desired application – essentially, just like for liquid electrolytes.

The continuously rising demand for electrochemical energy storage solutions has triggered extensive research in the field of batteries, especially in the last two decades.[1–4] Besides conventional lithium-ion batteries, which are - despite their remaining challenges - still setting the standard today,[1,3,5] the field of solid-state lithium-metal batteries has extensively emerged during the last years.[6–8] While the inherently higher safety of these systems seems to be especially interesting for consumer electronics and electric vehicles (EVs),[5] the possibility to use metallic lithium instead of graphite at the negative electrode might simultaneously pave the way to higher energy densities.[9–11]

Besides inorganic solid-state electrolytes such as oxide or thiophosphate materials, polymer electrolytes have attracted substantial attention owing to the manifold versatility of polymer structures, offering a great variety to optimize and tailor the properties of these electrolyte systems.[12–19] A common strategy to exploit this characteristic feature is the synthesis of block copolymers, consisting of a soft block to facilitate the transport of the Li^+ ions accompanied by a more rigid block to enhance the mechanical properties of the polymer.[20–22] One very well studied example is the SEO polymer (poly(ethylene oxide)-*b*-poly(styrene)), first presented and comprehensively investigated by Balsara and coworkers.[23–28] However, the Li^+ transference number of these systems remains low ($0.1 < t_{Li^+} < 0.3$), evidencing that charge transport is still mainly dominated by the electrochemically inactive anion.[29–32] Moreover, reversed cell polarization effects caused by (extensive) anion concentration gradients potentially lead to undesired side reactions and severe fading of the whole battery system.[33] To overcome these issues, researchers have introduced the concept of so-called 'single-ion conductors' (SICs) or 'ionomers',[20,34,35] which already bring along the conducting salt in the shape of a lithium cation weakly coordinated to an anionic moiety, which is covalently tethered to the polymer backbone.[36,37] Therefore, the charge transport in the electrolyte is carried by electrochemically active Li^+ only,

leading to highly effective charge transport, which is reflected by a Li^+ transference number approaching unity. On the other hand, the ionic conductivity of these (dry) materials is often limited and well below relevant performance indicators for large-scale applications.[38–40] Furthermore, modifications of the polymer backbone or synthesis of monomers containing the ionic function require more complicated synthesis procedures,[38–40] reducing their competitiveness in terms of manufacturing costs compared to regular polymer electrolytes or even liquid electrolyte[5] systems. However, recent theoretical calculations show that a conductivity of 0.4 mS cm^{-1} is already sufficient for EV applications due to the outstandingly high efficiency of charge transport in SICs.[41]

Very recently, Nguyen et al.[42] presented a new approach for the realization of single-ion conducting polymer electrolytes by polymerizing two different blocks of a poly(arylene ether sulfone) system to yield a lithium-containing multi-block copolymer electrolyte by attaching TFSI-like side chains to the backbone. High mechanical stability (provided by the rigid polymer backbone) allowed for the realization of self-standing membranes with excellent thermal and electrochemical stability, accompanied by very attractive ionic conductivities when swollen with so-called "molecular transporters" such as ethylene carbonate (EC) or propylene carbonate (PC).[42–44] Remarkably, Li‖NMC_{622}[44] and Li‖NMC_{811}[43] cells could be cycled for several hundred cycles with anodic cut-off voltages up to 4.5 V and temperatures ranging from 0 to 60 °C. However, the high fluorine content might be critical, as highly fluorinated molecules are usually associated with an increase in synthesis efforts/costs, reduced recycling capability (e.g., owing to the risk of generating toxic and corrosive HF),[45,46] as well as sustainability in general due to the low biodegradability.[47,48] While the fluorination of the side chain appears to be critical for ensuring a facile dissociation of the Li^+ cation owing to the electron-withdrawing effect on the anionic amide function,[49] the fluorination of the polymer backbone might be of lesser importance. To investigate this, we designed a multi-block copolymer electrolyte following the earlier studies but providing a completely fluorine-free backbone.

The chemical structure of this new SIC multi-block copolymer electrolyte (SIC-BCE) is presented in **Scheme 1**. Detailed information on the synthesis accompanied by the corresponding NMR spectra is provided in the Supporting Information (**Figure S1-S7**). The synthesis of the sidechain and its grafting to the non-fluorinated polymer backbone were essentially the same as reported for the fluorinated analogue.[42] However, a dibrominated 4,4'-difluorodiphenyl sulfone monomer was used to assemble the backbone of the ionophilic part of the polymer electrolyte. Therefore, the necessity of performing an additional bromination step after the polymerization reaction as for the SIC-BCE with fluorinated backbone could be omitted. Compared to the SIC-BCE with a fluorinated backbone, the ionic sidechain was tethered to the diphenyl sulfone unit instead of the biphenyl unit for synthetic reasons, as explained in detail in the Supporting Information.

To characterize the SIC-BCE, thermogravimetric analysis (TGA), differential scanning calorimetry (DSC), and gel permeation chromatography (GPC) were conducted. The dry membrane is stable up to more than 300 °C (**Figure 1a**) and two glass transition temperatures at around 160 °C and 220 °C (inset in **Figure 1a**). Moreover, the phase separation of the ionophilic block (carrying the Li^+ cation containing side chain) and the ionophobic block (providing mechanical stability) was confirmed by small-angle X-ray scattering (SAXS), revealing a domain spacing of around 33 nm (**Figure 1b**). The GPC results (**Table S1**) provided molecular weights of about 250,000 g mol^{-1} for M_n as well as 600,000 g mol^{-1} for M_w. Interestingly, these values are very similar to those reported for the polymer with a fluorinated backbone (see **Figure S8** for the chemical structure). The T_g values only slightly with around 150 and 220 °C, while the thermal stability, molecular weight, and domain spacing (ca. 40 nm) were essentially the same. These findings evidence that the thermal properties are predominately dictated by the existence of the poly(arylene ether sulfone) backbone and only marginally by the fluorination of one of the monomers.

To yield suitable ionic conductivities, varying amounts of EC were introduced into the ionomer membranes. This procedure yields more flexible and, depending on the EC content, also stickier membranes, while the self-standing properties were well maintained. Subsequently, electrochemical impedance spectroscopy was conducted for the SIC-BCE membranes with a varying EC content, ranging from 30% to 80% (all EC contents in wt.%), to determine the ionic conductivity in the temperature range from 10 °C to 90 °C (**Figure 2a**). Generally, the conductivity increased with increasing temperature and EC content. Values beyond 1 mS cm^{-1} at slightly elevated temperatures (45 °C) were found for an EC content of 60% (and higher). At the same time, however, a sudden drop in conductivity was observed for EC contents beyond 50% when the temperature decreased below 20 °C. This behavior is assigned to the presence of free EC clusters at such elevated EC contents beyond a certain threshold up to which the EC molecules are selectively coordinating the ionophilic domains.[42] These clusters of free EC are solidifying at temperatures well below the melting point of EC (ca. 36 °C), which leads to a substantial decrease in conductivity, presumably due to a blocking of the ionophilic charge transport pathways, not observed for lower EC concentrations. Nonetheless, this effect is reversible. When increasing the temperature again, the EC clusters melt, and the conductivity recovers to the same values observed before. This behavior was further elucidated by DSC measurements of EC-containing membranes (**Figure 2b**). While no traces of free EC were observed for an EC content of 20%, a membrane with 50% EC already showed a minor peak at the melting temperature of EC. Accordingly, these minor concentrations of clustered EC were not large enough to cause the observed drop in ionic conductivity at low temperatures.[42] At 60% EC, however, the observed melting of free EC correlates with a drop in ionic conductivity beyond the melting point of EC, indicating that such elevated EC content is sufficient to block the ionophilic charge transport pathways. Similar observa-

tions were made for the polymer with partially fluorinated backbone in DSC and conductivity measurements.[42] Remarkably, the ionic conductivity seems to be affected only marginally by the absence of fluorine in the backbone. In fact, even slightly higher conductivities were observed for the SIC-BCE with the non-fluorinated polymer backbone.

For the further studies, SIC-BCE membranes with an EC content of 65% were used, which are a good compromise between a maximized ionic conductivity and maintaining mechanically suitable properties that facilitate handling and processing.

The electrochemical characterization of these SIC-BCE membranes is presented in **Figure 3**. The lithium stripping/plating test at varying current densities (**Figure 3a**) reveals stable lithium cycling up to a current density of 50 μA cm^{-2} and an increasing overpotential at 100 μA cm^{-2}. The magnification of the stripping/plating cycles at 10 μA cm^{-2} (**Figure 3b**) shows the rectangular shape voltage response, characteristic for a single-ion conductor without a noticeable concentration gradient. At elevated current density (i.e., 100 μA cm^{-2}), however, the voltage response shows an increasing overpotential and a non-perfectly flat voltage response. While such behavior is commonly assigned to the build-up of a charge concentration gradient in dual-ion electrolytes, such behavior is theoretically not expected for SIC polymer electrolytes (SIC-PEs), where the anionic charge is covalently tethered to the polymer backbone and, thus, immobile. According to Borzutzki et al.[50] this behavior indicates the limited charge transport across the electrode|electrolyte interphase, which becomes the bottleneck at certain current densities. Hence, this finding might indicate a rather resistive interphase formed in the present case. When applying a current density of 50 μA cm^{-2}, though, the constant-current long-term lithium stripping/plating shows a rather stable overpotential with only a marginal rise during over 1,000 h (**Figure 3c**). No indication of a short circuit or (soft) dendrite formation was observed. The determination of the electrochemical stability window (ESW, **Figure 3d**) shows a continuous increase in (negative) current below 0 V during the cathodic sweep, which is assigned to the plating of metallic lithium. The broad peak at around 1 V is attributed to the reductive decomposition of EC and, potentially, DMSO traces remaining in the membrane from the casting process.[42] The anodic sweep reveals a small peak at around 4.5 V, which might similarly originate from DMSO traces and/or an initial oxidative decomposition of EC, forming a passivating film at the electrode|electrolyte interface, while the continuously rising current at further elevated potentials indicates the ongoing oxidation of the SIC-BCE. Compared to the SIC-BCE with the fluorinated backbone, the electrochemical performance of the fluorine-free analogue reveals considerable differences. In that case, a stable overpotential for the lithium stripping/plating experiments was observed up to a current density of 500 μA cm^{-2}.[42] As the ionic conductivity was comparable, this finding might be related to different charge-transfer processes across the electrode|electrolyte interface, resulting from a different chemical composition of the interphase formed between the two phases. Additionally, the electrochemical stability towards oxidation is slightly lower compared to analogue SIC-BCE with the fluorinated backbone, i.e., 4.5 vs. 4.8 V. Both findings suggest that the presence of fluorine in the backbone is decisive for the interfacial stability and the composition of the interphases formed.

To gain deeper insights into the impact of the fluorinated backbone, two model compounds were identified that well resemble the (non-)fluorinated arylene ether building block of the polymer backbone, which is considered the most sensitive part of the polymer towards reduction/oxidation: diphenyl ether (DPE) and decafluorodiphenyl ether (DFDPE). The two model compounds were dissolved in an electrolyte consisting of acetonitrile and tetra n-butylammonium tetrafluoroborate (TnBATFB) as the conducting salt to provide a suitable experimental setup. Both electrolyte compositions were studied in 3-electrode cells with a platinum working electrode and activated carbon as counter and reference electrodes. The results are displayed in **Figure 4**. The electrolyte containing DFDPE shows a slightly higher stability towards reduction compared to DPE, while both reveal a higher stability than the pure electrolyte (**Figure 4a**), presumably due to stabilizing effects of the model compounds. The impact of the fluorination becomes even more apparent upon oxidation, revealing superior stability of the DFDPE-comprising electrolyte solution (**Figure 4b**). While the DPE-containing electrolyte is already oxidized at around 4.5 V vs. Li^+/Li, the DFDPE-comprising electrolyte is stable up to 5.4 V vs. Li^+/Li. The value of 4.5 V observed for DPE matches exceptionally well with the oxidation stability of the polymer electrolyte (**Figure 3d**). To further confirm this finding, DFT calculations were performed to theoretically determine the electrochemical stability window of the two model compounds (**Figure 4c**). The results are well in line with the experimental findings (**Figure 4d**), yielding a stability window of -0.5 to 5.8 V for DFDPE, which is substantially broader than the one found for DPE with 0.1 to 4.8 V. Only the reduction potential of DFDPE seems to be slightly underestimated in the experiment (**Figure 4d**), most likely due to different dielectric constants of pure acetonitrile used for the simulations and the acetonitrile-salt mixture employed in the experimental setup. To ensure comparability of the measurement in acetonitrile with the real EC environment in the membranes, the reduction/oxidation potential of the two model compounds in EC was calculated as well (**Table S2**). Minor discrepancies were found to be within the error of the determination of the absolute potential of the hydrogen electrode (±0.2 V) and were therefore neglected. Generally, the results unambiguously highlight the superior electrochemical stability of the fluorinated aromatic ether bond owing to the electron-withdrawing effect of fluorine.

While these findings provide an explanation for the different electrochemical stability towards oxidation, the difference concerning the stability towards lithium metal, as observed for the lithium stripping/plating experiments, remains to be understood. For this purpose, lithium metal was exposed to the two model compounds – either in liquid DPE or a solution of (solid) DFDPE in DPE – and subsequently investigated by X-ray photoelectron spectroscopy (XPS) (**Figure 5**). The detail spectra in the

F 1s region (**Figure 5a**) clearly demonstrate the extensive formation of LiF in the case of DFDPE (peak at ~685 eV). Remarkably, though, the presence of a smaller amount of LiF is also detected for pristine and DPE-treated lithium, most likely originating from the contact with non-sticky fluoropolymers such as PTFE during the manufacturing process. Essentially the same trend is observed for the peak related to CF_x species (peak at ~688 eV, which is much more intense for the DFDPE-treated lithium. The observation that it is lower for the DPE-treated lithium than for the pristine lithium suggests that such species, resulting from the contact with fluorinated polymers during the processing, might be washed away in DPE to a certain extent. The broad signals observed in the Li 1*s* spectra (**Figure 5b**) include contributions from different lithium compounds such as Li_2O, Li_2CO_3 or LiF originating from the processing of the lithium metal.[51] With regard to peak position and intensity, the Li 1s spectrum of the lithium metal exposed to DPE is essentially the same as the one recorded for the pristine lithium, while the intensity of the spectrum obtained for the DFDPE(+DPE)-treated lithium grows slightly and the maximum shows a slight shift to higher binding energies. This shift is attributed to the larger contribution of LiF which has a higher binding energy (55.6 eV) than, e.g., Li_2CO_3 (55.2 eV). The comparison of the C 1s spectra (**Figure 5c**) shows that the content of carbonaceous species (C-H) is much smaller for the DFDPE sample than for the two others, i.e., the surface layer of the latter two samples contains much more organic species. The O 1s spectra (**Figure 5d**) are essentially in line with the observations from the other detail spectra. In sum, these results clearly evidence the formation of a LiF-rich interphase on lithium in the presence of DFDPE, which is beneficial for the application of high current densities on lithium-metal electrodes and the realization of a stable electrode|electrolyte interphase, as reported for the fluorine-containing SIC-BCE backbone compared to the fluorine-free backbone presented herein.

In conclusion, we present the successful synthesis of a nanostructured SIC-BCE based on a completely fluorine-free polymer backbone. This SIC-BCE offers a very high ionic conductivity of >1 mS cm^{-1} at slightly elevated temperatures and a suitable electrochemical stability, as determined by LSV. However, the absence of fluorine in the backbone results in a slightly lower stability towards oxidation, owing to the absence of the stabilizing electron-withdrawing effect on the ether bond, and affects the composition of the interphase formed on the lithium-metal electrode, being dominated by organic species rather than LiF. Such LiF-poor interphase appears detrimental to the charge transfer across the lithium|SIC-BCE interphase, limiting the maximum current density that can be applied without observing the build-up of a concentration gradient and an increasing polarization. As this might be "healed", e.g., by the application of suitable coatings on metallic lithium, these findings are anticipated to support the tailored development of polymer electrolytes with fine-tuned physicochemical and electrochemical properties for specific battery cell chemistries, while potentially allowing for an improved sustainability and lower cost, when the electrochemical stability and interphase formation are less critical or can be optimized by complementary approaches.

ASSOCIATED CONTENT

Supporting Information. Synthesis procedures, NMR spectra, membrane preparation, characterization methods, details on the DFT simulation, GPC results, overpotential inset, and SAXS pattern. This material is available free of charge via the Internet at http://pubs.acs.org.

AUTHOR INFORMATION

Corresponding Authors

* Dominic Bresser – Karlsruhe Institute of Technology, Helmholtz Institute Ulm, Helmholtzstrasse 11, 89081 Ulm, Germany; https://orcid.org/0000-0001-6429-6048; dominic.bresser@kit..edu

* Stefano Passerini – Karlsruhe Institute of Technology, Helmholtz Institute Ulm, Helmholtzstrasse 11, 89081 Ulm, Germany; https://orcid.org/0000-0002-6606-5304; stefano.passerini@kit.edu

* Cristina Iojoiu – Univ. Grenoble Alpes, Univ. Savoie Mont Blanc, CNRS, Grenoble INP (Institute of Engineering Univ. Grenoble Alpes), LEPMI, UMR5279, 38000, Grenoble, France; https://orcid.org/0000-0002-5823-8025; Email: cristina.iojoiu@grenoble-inp.fr

Present Address

† Alessandro Mariani – Department of Science and Engineering of Materials, Environment, and Urban Planning (SIMAU), Università Politecnica delle Marche, 60131 Ancona, Italy.

Huu-Dat Nguyen - R&D Center, Automotive Cells Company (ACC), 136 quater, Avenue d'Aquitaine, 33520 Bruges, France.

Author Contributions

The manuscript was written through contributions of all authors. All authors have given approval to the final version of the manuscript.

Funding Sources

The authors would like to thank the Federal Ministry for Education and Research (BMBF) for financial support within the FestBatt (03XP0175B) and FB2-POLY (03XP0429B) project. Financial support from the Helmholtz Association is also kindly acknowledged. Furthermore, financial support by the French National Research Agency within the NSPEM project (ANR-16-CE05-0016), and the Centre of Excellence of Multifunctional Architectured Materials "CEMAM" (AN-10-LABX-44–01) are gratefully acknowledged.

Notes

The authors declare no conflict of interest.

ACKNOWLEDGMENT

Dr. Peter Ruschhaupt (KIT, HIU) is gratefully acknowledged for providing carbon electrodes used for the electrochemical measurements on the model compounds. Moreover, the authors would like to thank Dr. Alberto Varzi (KIT, HIU) for the helpful discussion of the experimental setups and results. The von Delius group at Ulm University is kindly acknowledged for NMR service measurements.

REFERENCES

(1) Tarascon, J. M.; Armand, M. Issues and Challenges Facing Rechargeable Lithium Batteries. *Nature* **2001**, *414* (6861), 359–367.

(2) Tarascon, J. M. Key Challenges in Future Li-Battery Research. *Philos. Trans. R. Soc. A Math. Phys. Eng. Sci.* **2010**, *368* (1923), 3227–3241.

(3) Armand, M.; Axmann, P.; Bresser, D.; Copley, M.; Edström, K.; Ekberg, C.; Guyomard, D.; Lestriez, B.; Novák, P.; Petranikova, M.; Porcher, W.; Trabesinger, S.; Wohlfahrt-Mehrens, M.; Zhang, H. Lithium-Ion Batteries – Current State of the Art and Anticipated Developments. *J. Power Sources* **2020**, *479*, 228708.

(4) Dunn, B.; Kamath, H.; Tarascon, J. M. Electrical Energy Storage for the Grid: A Battery of Choices. *Science* **2011**, *334* (6058), 928–935.

(5) Kalhoff, J.; Eshetu, G. G.; Bresser, D.; Passerini, S. Safer Electrolytes for Lithium-Ion Batteries: State of the Art and Perspectives. *ChemSusChem* **2015**, *8* (13), 2154–2175.

(6) Manthiram, A.; Yu, X.; Wang, S. Lithium Battery Chemistries Enabled by Solid-State Electrolytes. *Nat. Rev. Mater.* **2017**, *2* (4), 1–16.

(7) Fan, L.; Wei, S.; Li, S.; Li, Q.; Lu, Y. Recent Progress of the Solid-State Electrolytes for High-Energy Metal-Based Batteries. *Adv. Energy Mater.* **2018**, *8* (11), 1702657.

(8) Mauger, A.; Julien, C. M.; Paolella, A.; Armand, M.; Zaghib, K. Building Better Batteries in the Solid State: A Review. *Materials* **2019**, *12* (23), 1–85.

(9) Xu, W.; Wang, J.; Ding, F.; Chen, X.; Nasybulin, E.; Zhang, Y.; Zhang, J. G. Lithium Metal Anodes for Rechargeable Batteries. *Energy Environ. Sci.* **2014**, *7* (2), 513–537.

(10) Lin, D.; Liu, Y.; Cui, Y. Reviving the Lithium Metal Anode for High-Energy Batteries. *Nat. Nanotechnol.* **2017**, *12* (3), 194–206.

(11) Cheng, X.-B.; Zhang, R.; Zhao, C.-Z.; Zhang, Q. Toward Safe Lithium Metal Anode in Rechargeable Batteries: A Review. *Chem. Rev.* **2017**, *117* (15), 10403–10473.

(12) Quartarone, E.; Mustarelli, P. Electrolytes for Solid-State Lithium Rechargeable Batteries: Recent Advances and Perspectives. *Chem. Soc. Rev.* **2011**, *40* (5), 2525–2540.

(13) Di Noto, V.; Lavina, S.; Giffin, G. A.; Negro, E.; Scrosati, B. Polymer Electrolytes: Present, Past and Future. *Electrochim. Acta* **2011**, *57* (1), 4–13.

(14) Hallinan, D. T.; Balsara, N. P. Polymer Electrolytes. *Annu. Rev. Mater. Res.* **2013**, *43* (1), 503–525.

(15) Wang, J.; Li, S.; Zhao, Q.; Song, C.; Xue, Z. Structure Code for Advanced Polymer Electrolyte in Lithium-Ion Batteries. *Adv. Funct. Mater.* **2021**, *31* (12), 1–35.

(16) Xi, G.; Xiao, M.; Wang, S.; Han, D.; Li, Y.; Meng, Y. Polymer-Based Solid Electrolytes: Material Selection, Design, and Application. *Adv. Funct. Mater.* **2021**, *31* (9), 1–28.

(17) Bresser, D.; Lyonnard, S.; Iojoiu, C.; Picard, L.; Passerini, S. Decoupling Segmental Relaxation and Ionic Conductivity for Lithium-Ion Polymer Electrolytes. *Mol. Syst. Des. Eng.* **2019**, *4* (4), 779–792.

(18) Choo, Y.; Halat, D. M.; Villaluenga, I.; Timachova, K.; Balsara, N. P. Diffusion and Migration in Polymer Electrolytes. *Prog. Polym. Sci.* **2020**, *103*, 101220.

(19) Bocharova, V.; Sokolov, A. P. Perspectives for Polymer Electrolytes: A View from Fundamentals of Ionic Conductivity. *Macromolecules* **2020**, *53* (11), 4141–4157.

(20) Mayer, A.; Steinle, D.; Passerini, S.; Bresser, D. Block Copolymers as (Single-Ion Conducting) Lithium Battery Electrolytes. *Nanotechnology* **2021**, *33* (6), 62002.

(21) Young, W. S.; Kuan, W. F.; Epps, T. H. Block Copolymer Electrolytes for Rechargeable Lithium Batteries. *J. Polym. Sci. Part B Polym. Phys.* **2014**, *52* (1), 1–16.

(22) Liu, T.; Liu, G. Block Copolymers for Supercapacitors, Dielectric Capacitors and Batteries. *J. Phys. Condens. Matter* **2019**, *31* (23), 1–27.

(23) Singh, M.; Odusanya, O.; Wilmes, G. M.; Eitouni, H. B.; Gomez, E. D.; Patel, A. J.; Chen, V. L.; Park, M. J.; Fragouli, P.; Iatrou, H.; Hadjichristidis, N.; Cookson, D.; Balsara, N. P. Effect of Molecular Weight on the Mechanical and Electrical Properties of Block Copolymer Electrolytes. *Macromolecules* **2007**, *40* (13), 4578–4585.

(24) Wanakule, N. S.; Panday, A.; Mullin, S. A.; Gann, E.; Hexemer, A.; Balsara, N. P. Ionic Conductivity of Block Copolymer Electrolytes in the Vicinity of Order-Disorder and Order-Order Transitions. *Macromolecules* **2009**, *42* (15), 5642–5651.

(25) Yuan, R.; Teran, A. A.; Gurevitch, I.; Mullin, S. A.; Wanakule, N. S.; Balsara, N. P. Ionic Conductivity of Low Molecular Weight Block Copolymer Electrolytes. *Macromolecules* **2013**, *46* (3), 914–921.

(26) Thelen, J. L.; Teran, A. A.; Wang, X.; Garetz, B. A.; Nakamura, I.; Wang, Z. G.; Balsara, N. P. Phase Behavior of a Block Copolymer/Salt Mixture through the Order-to-Disorder Transition. *Macromolecules* **2014**, *47* (8), 2666–2673.

(27) Loo, W. S.; Galluzzo, M. D.; Li, X.; Maslyn, J. A.; Oh, H. J.; Mongcopa, K. I.; Zhu, C.; Wang, A. A.; Wang, X.; Garetz, B. A.; Balsara, N. P. Phase Behavior of Mixtures of Block Copolymers and a Lithium Salt. *J. Phys. Chem. B* **2018**, *122* (33), 8065–8074.

(28) Hallinan, D. T.; Mullin, S. A.; Stone, G. M.; Balsara, N. P. Lithium Metal Stability in Batteries with Block Copolymer Electrolytes. *J. Electrochem. Soc.* **2013**, *160* (3), A464–A470.

(29) Timachova, K.; Watanabe, H.; Balsara, N. P. Effect of Molecular Weight and Salt Concentration on Ion Transport and the Transference Number in Polymer Electrolytes. *Macromolecules* **2015**, *48* (21), 7882–7888.

(30) Pesko, D. M.; Timachova, K.; Bhattacharya, R.; Smith, M. C.; Villaluenga, I.; Newman, J.; Balsara, N. P. Negative Transference Numbers in Poly(Ethylene Oxide)-Based Electrolytes. *J. Electrochem. Soc.* **2017**, *164* (11), E3569–E3575.

(31) Villaluenga, I.; Pesko, D. M.; Timachova, K.; Feng, Z.; Newman, J.; Srinivasan, V.; Balsara, N. P. Negative Stefan-Maxwell Diffusion Coefficients and Complete Electrochemical Transport Characterization of Homopolymer and Block Copolymer Electrolytes. *J. Electrochem. Soc.* **2018**, *165* (11), A2766–A2773.

(32) Villaluenga, I.; Inceoglu, S.; Jiang, X.; Chen, X. C.; Chintapalli, M.; Wang, D. R.; Devaux, D.; Balsara, N. P. Nanostructured Single-Ion-Conducting Hybrid Electrolytes Based on Salty Nanoparticles and Block Copolymers. *Macromolecules* **2017**, *50* (5), 1998–2005.

(33) Helen Wang, J. H.; Colby, R. H. Exploring the Role of Ion Solvation in Ethylene Oxide Based Single-Ion Conducting Polyanions and Polycations. *Soft Matter* **2013**, *9* (43), 10275–10286.

(34) Zhang, H.; Li, C.; Piszcz, M.; Coya, E.; Rojo, T.; Rodriguez-Martinez, L. M.; Armand, M.; Zhou, Z. Single Lithium-Ion Conducting Solid Polymer Electrolytes: Advances and Perspectives. *Chem. Soc. Rev.* **2017**, *46* (3), 797–815.

(35) Strauss, E.; Menkin, S.; Golodnitsky, D. On the Way to High-Conductivity Single Lithium-Ion Conductors. *J. Solid State Electrochem.* **2017**, *21* (7), 1879–1905.

(36) Sadoway, D. R.; Huang, B.; Trapa, P. E.; Soo, P. P.; Bannerjee, P.; Mayes, A. M. Self-Doped Block Copolymer Electrolytes for Solid-State, Rechargeable Lithium Batteries. *J. Power Sources* **2001**, *97–98*, 621–623.

(37) Ryu, S. W.; Trapa, P. E.; Olugebefola, S. C.; Gonzalez-Leon, J. A.; Sadoway, D. R.; Mayes, A. M. Effect of Counter Ion Placement on Conductivity in Single-Ion Conducting Block Copolymer Electrolytes. *J. Electrochem. Soc.* **2005**, *152* (1), A158–A163.

(38) Bouchet, R.; Maria, S.; Meziane, R.; Aboulaich, A.; Lienafa, L.; Bonnet, J.-P.; Phan, T. N. T.; Bertin, D.; Gigmes, D.; Devaux, D.; Denoyel, R.; Armand, M. Single-Ion BAB Triblock Copolymers as Highly Efficient Electrolytes for Lithium-Metal Batteries. *Nat. Mater.* **2013**, *12* (5), 452–457.

(39) Porcarelli, L.; Aboudzadeh, M. A.; Rubatat, L.; Nair, J. R.; Shaplov, A. S.; Gerbaldi, C.; Mecerreyes, D. Single-Ion Triblock Copolymer Electrolytes Based on Poly(Ethylene Oxide) and Methacrylic Sulfonamide Blocks for Lithium Metal Batteries. *J. Power Sources* **2017**, *364*, 191–199.

(40) Devaux, D.; Liénafa, L.; Beaudoin, E.; Maria, S.; Phan, T. N. T.;

Gigmes, D.; Giroud, E.; Davidson, P.; Bouchet, R. Comparison of Single-Ion-Conductor Block-Copolymer Electrolytes with Polystyrene-TFSI and Polymethacrylate-TFSI Structural Blocks. *Electrochim. Acta* **2018**, *269*, 250–261.

(41) Kim, H.-K.; Srinivasan, V. Status and Targets for Polymer-Based Solid-State Batteries for Electric Vehicle Applications. *J. Electrochem. Soc.* **2020**, *167* (13), 130520.

(42) Nguyen, H. D.; Kim, G. T.; Shi, J.; Paillard, E.; Judeinstein, P.; Lyonnard, S.; Bresser, D.; Iojoiu, C. Nanostructured Multi-Block Copolymer Single-Ion Conductors for Safer High-Performance Lithium Batteries. *Energy Environ. Sci.* **2018**, *11* (11), 3298–3309.

(43) Chen, Z.; Steinle, D.; Nguyen, H. D.; Kim, J. K.; Mayer, A.; Shi, J.; Paillard, E.; Iojoiu, C.; Passerini, S.; Bresser, D. High-Energy Lithium Batteries Based on Single-Ion Conducting Polymer Electrolytes and Li[Ni0.8Co0.1Mn0.1]O2 Cathodes. *Nano Energy* **2020**, *77*, 105129.

(44) Steinle, D.; Chen, Z.; Nguyen, H. D.; Kuenzel, M.; Iojoiu, C.; Passerini, S.; Bresser, D. Single-Ion Conducting Polymer Electrolyte for Li||LiNi0.6Mn0.2Co0.2O2 Batteries—Impact of the Anodic Cutoff Voltage and Ambient Temperature. *J. Solid State Electrochem.* **2022**, *26*, 97–102.

(45) Hernández, G.; Mindemark, J.; Naylor, A. J.; Chien, Y. C.; Brandell, D.; Edstrom, K. Elimination of Fluorination: The Influence of Fluorine-Free Electrolytes on the Performance of LiNi1/3Mn1/3Co1/3O2/Silicon-Graphite Li-Ion Battery Cells. *ACS Sustain. Chem. Eng.* **2020**, *8* (27), 10041–10052.

(46) Zheng, X.; Zhu, Z.; Lin, X.; Zhang, Y.; He, Y.; Cao, H.; Sun, Z. A Mini-Review on Metal Recycling from Spent Lithium Ion Batteries. *Engineering* **2018**, *4* (3), 361–370.

(47) European Chemicals Agency (ECHA), entry on LiTFSI (lithium bis(trifluoromethanesulfonyl) imide), CAS no: 90076-65-6. https://echa.europa.eu/brief-profile/-/briefprofile/100.101.430 (accessed 2021-12-30).

(48) Glüge, J.; Scheringer, M.; Cousins, I. T.; Dewitt, J. C.; Goldenman, G.; Herzke, D.; Lohmann, R.; Ng, C. A.; Trier, X.; Wang, Z. An Overview of the Uses of Per- And Polyfluoroalkyl Substances (PFAS). *Environ. Sci. Process. Impacts* **2020**, *22* (12), 2345–2373.

(49) Zhang, H.; Oteo, U.; Zhu, H.; Judez, X.; Martinez-Ibañez, M.; Aldalur, I.; Sanchez-Diez, E.; Li, C.; Carrasco, J.; Forsyth, M.; Armand, M. Enhanced Lithium-Ion Conductivity of Polymer Electrolytes by Selective Introduction of Hydrogen into the Anion. *Angew. Chemie - Int. Ed.* **2019**, *58* (23), 7829–7834.

(50) Borzutzki, K.; Nair, J. R.; Winter, M.; Brunklaus, G. Does Cell Polarization Matter in Single-Ion Conducting Electrolytes? *ACS Appl. Mater. Interfaces* **2022**, *14* (4), 5211–5222.

(51) Fujieda, T.; Yamamoto, N.; Saito, K.; Ishibashi, T.; Honjo, M.; Koike, S.; Wakabayashi, N.; Higuchi, S. Surface of Lithium Electrodes Prepared in Ar + CO2 Gas. *J. Power Sources* **1994**, *52* (2), 197–200.

Scheme 1. Chemical structure of the multi-block copolymer with a fluorine-free backbone; the ratio of the ionophilic and ionophobic block (n/m) was 1:1. The ion exchange capacity was determined to be 1.08 meq Li^+/g.

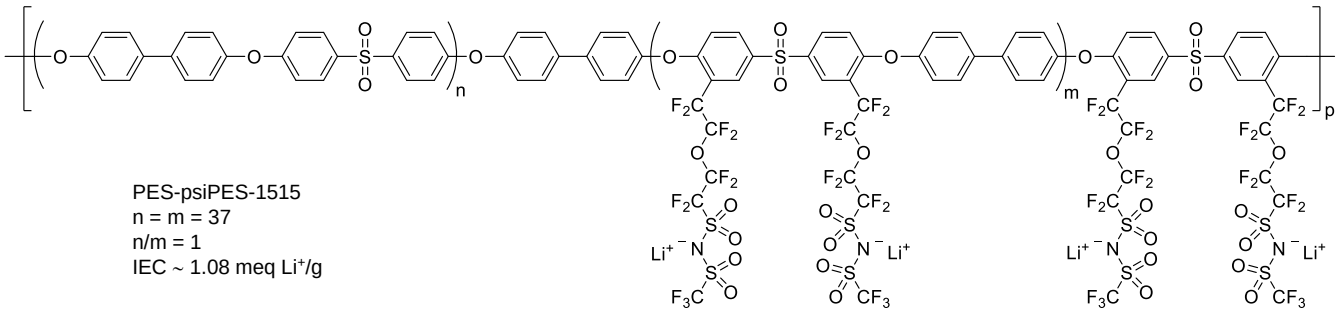

PES-psiPES-1515
n = m = 37
n/m = 1
IEC ~ 1.08 meq Li^+/g

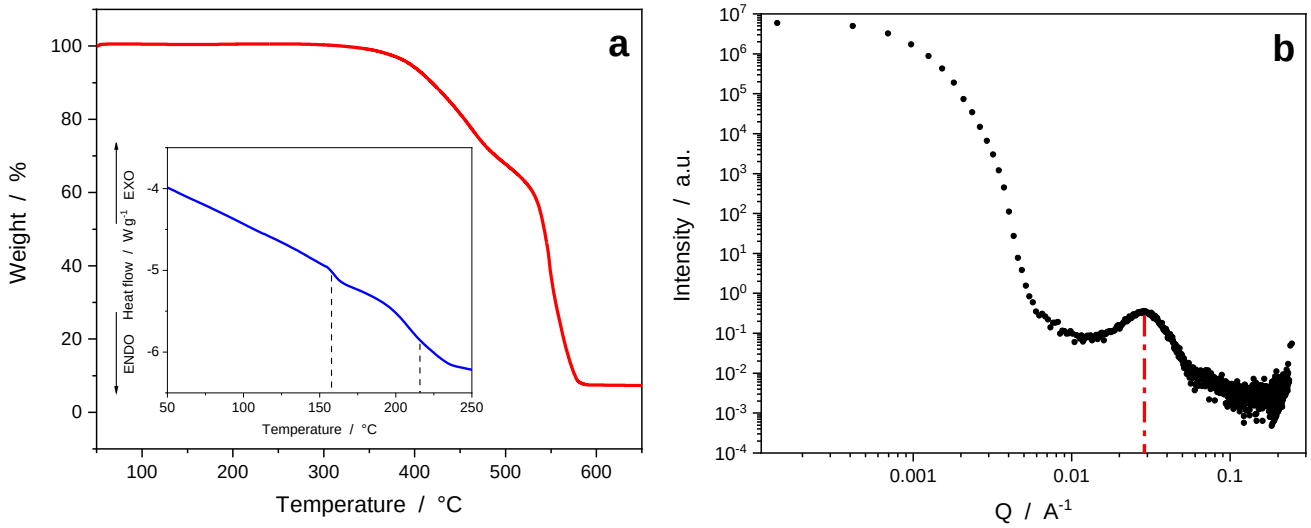

Figure 1. Physicochemical characterization of the dry ionomer by (a) TGA and DSC (provided as inset) as well as (b) SAXS with an indication of the correlation peak, evidencing the nano-structuration.

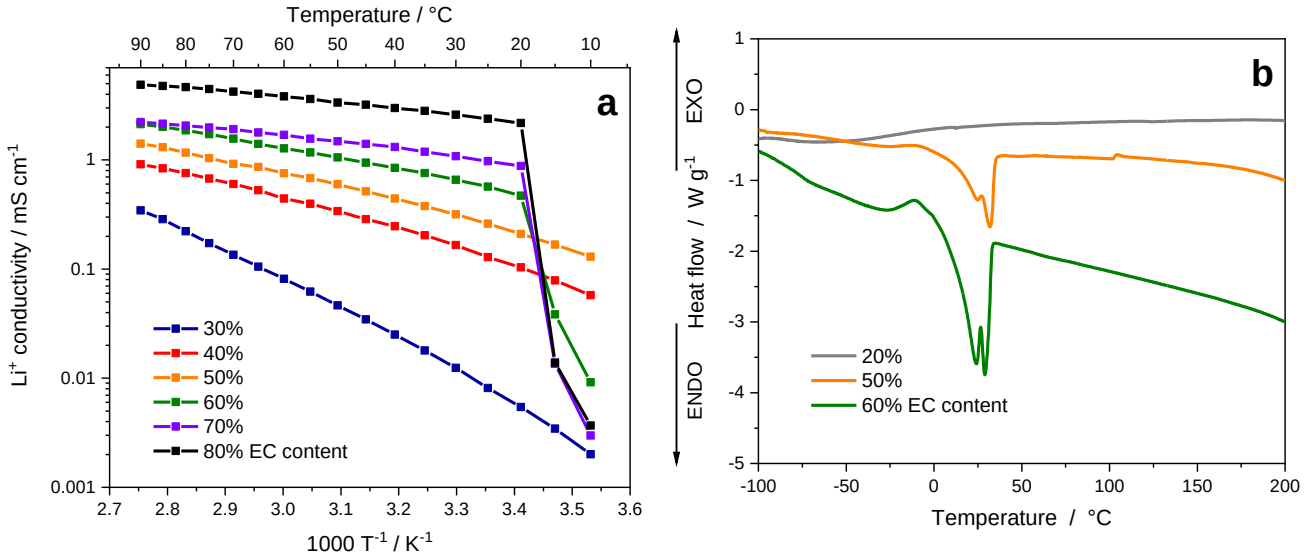

Figure 2. (a) Ionic conductivity of the SIC-BCEs as a function of temperature for varying EC contents. (b) DSC traces of the ionomer membranes with selected EC contents (i.e., 20%, 50% and 60% EC).

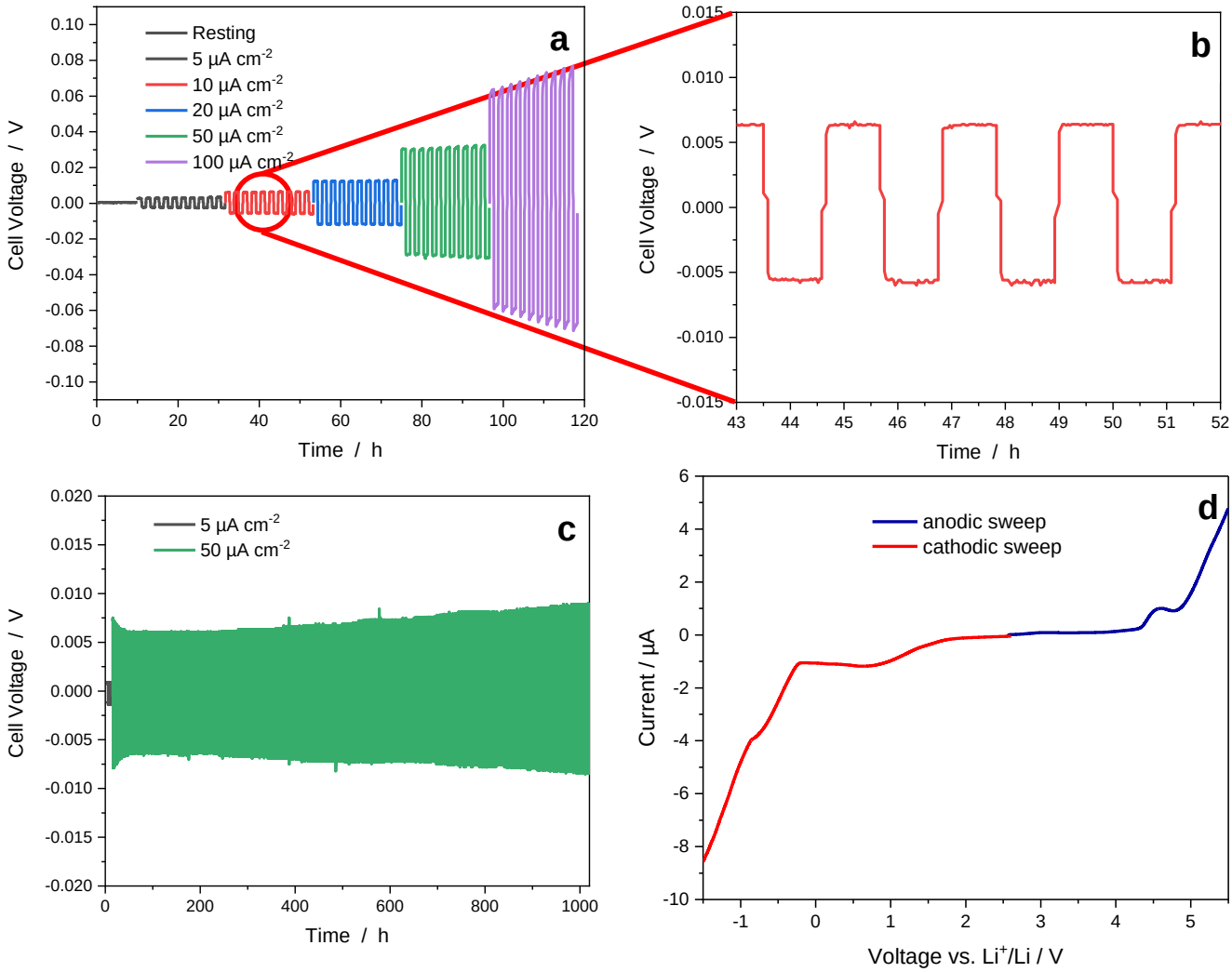

Figure 3. Electrochemical characterization of the SIC-BCE: (a) Lithium stripping/plating test at varying current densities (each current density was applied for ten cycles); (b) magnification of the stripping/plating cycles at 20 μA cm^{-2}, as highlighted in (a); (c) long-term lithium stripping/plating for more than 1000 h at 50 μA cm^{-2} after 5 cycles at 5 μA cm^{-2}; (d) determination of the electrochemical stability window via linear sweep voltammetry with the cathodic sweep in red and the anodic sweep in blue.

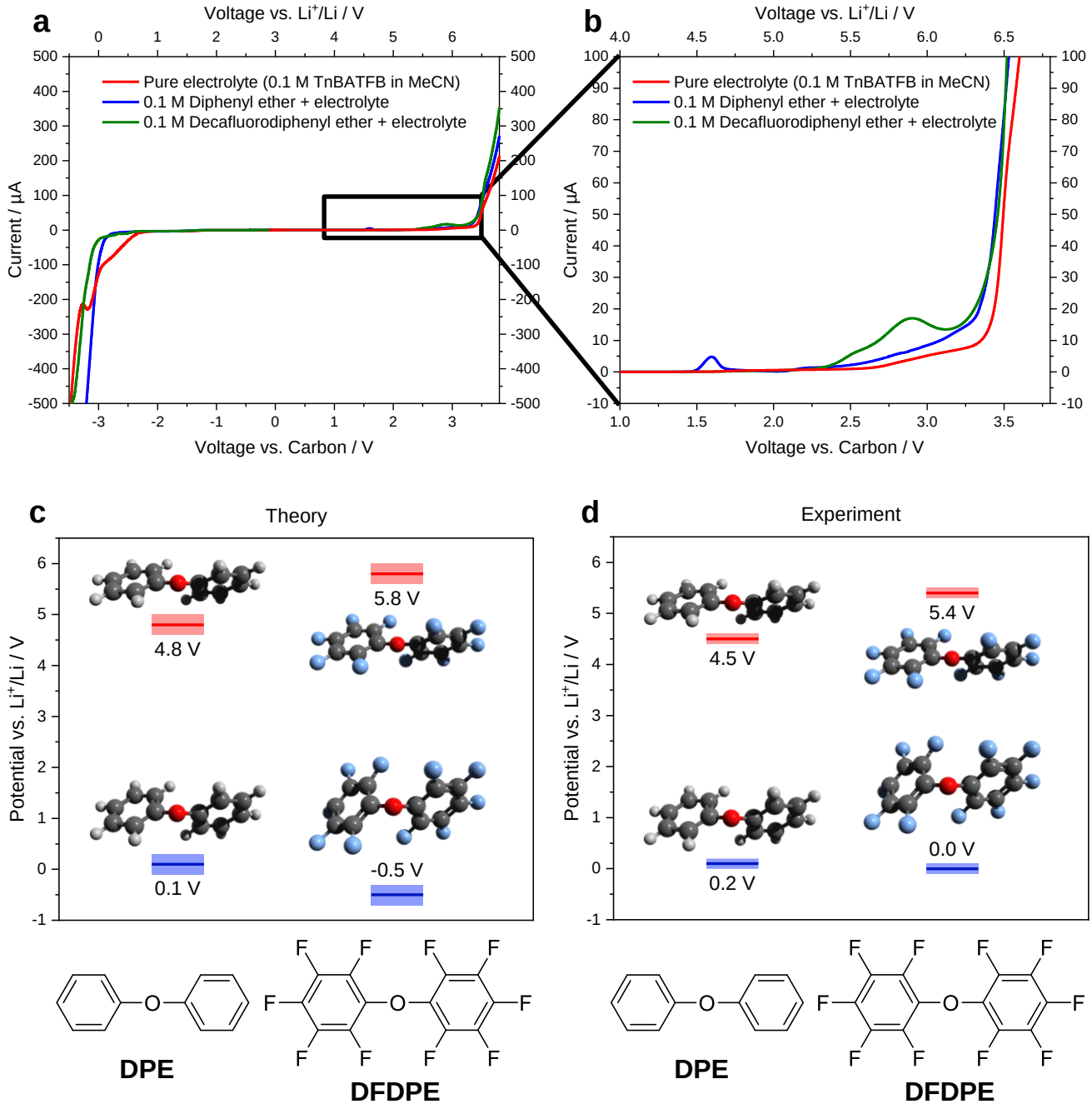

Figure 4. Investigation of the two model compounds DPE and DFDPE: (a) Experimentally determined electrochemical stability window in the supporting electrolyte (0.1 M TnBATFB in MeCN) with the electrochemical stability of the supporting electrolyte as reference; (b) magnification of the anodic sweep, as indicated in (a); (c) redox potentials of the two model compounds calculated via DFT in comparison with (d) the experimentally determined values (with the reduction potentials in blue and the oxidation potentials in red; the shaded regions indicate the error margins).

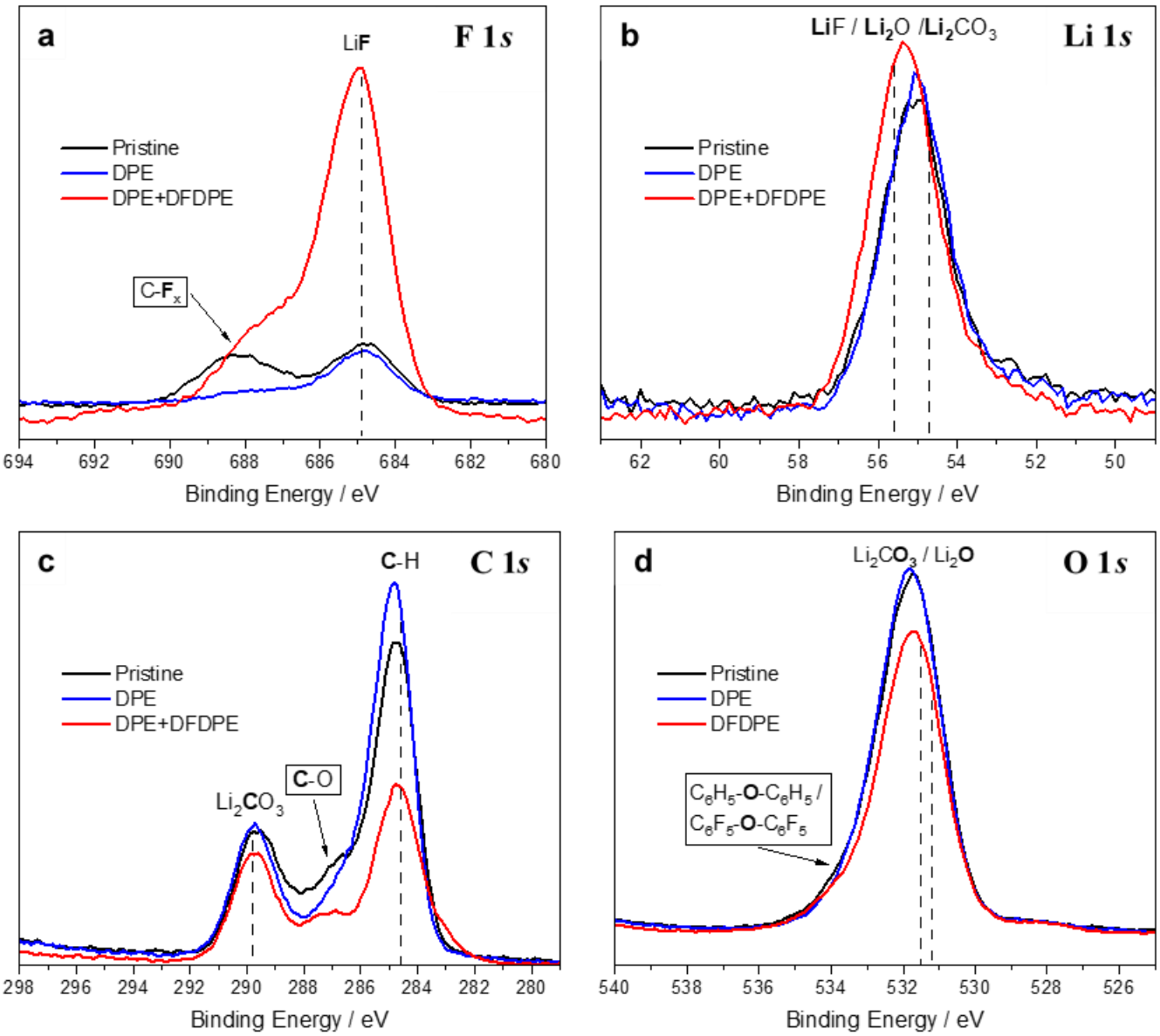

Figure 5. XPS analysis of a DPE-treated (blue) and a DFDPE+DPE-treated (red) lithium foil compared to a pristine lithium foil (black) serving as reference. Detail spectra in the (a) F 1s, (b) Li 1s, (c) C 1s, and (d) O 1s region.

Authors are required to submit a graphic entry for the Table of Contents (TOC) that, in conjunction with the manuscript title, should give the reader a representative idea of one of the following: A key structure, reaction, equation, concept, or theorem, etc., that is discussed in the manuscript. Consult the journal's Instructions for Authors for TOC graphic specifications.

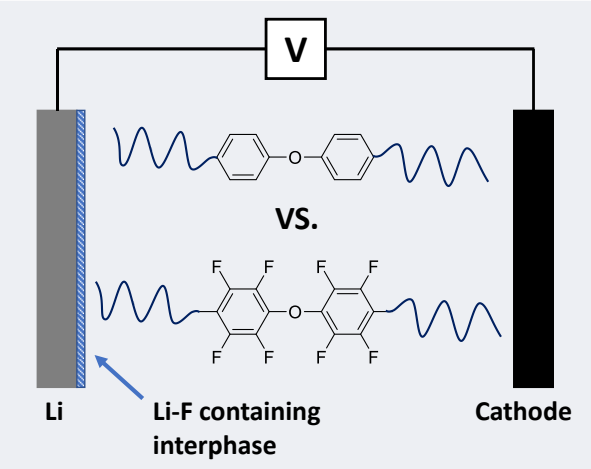

Insert Table of Contents artwork here

Supporting Information

Influence of Polymer Backbone Fluorination on the Electrochemical Behavior of Single-Ion Conducting Multi-Block Copolymer Electrolytes

Alexander Mayer[a,b], Huu-Dat Nguyen[c,#], Alessandro Mariani[a,b,†], Thomas Diemant[a,b], Cristina Iojoiu[c,d,*], Stefano Passerini[a,b,*], and Dominic Bresser[a,b,*]

[a] *Helmholtz Institute Ulm (HIU), Helmholtzstrasse 11, 89081 Ulm, Germany*
[b] *Karlsruhe Institute of Technology (KIT), P.O. Box 3640, 76021 Karlsruhe, Germany*
[c] *Univ. Grenoble Alpes, Univ. Savoie Mont Blanc, CNRS, Grenoble INP, LEPMI, UMR5279, 38000 Grenoble, France*
[d] *Réseau sur le Stockage Electrochimique de l'Energie (RS2E), CNRS FR3459, 80039 Amiens Cedex, France*

***Corresponding authors:**
dominic.bresser@kit.edu ; stefano.passerini@kit.edu ; cristina.iojoiu@grenoble-inp.fr

Present addresses:
[†] *Department of Science and Engineering of Materials, Environment, and Urban Planning (SIMAU), Università Politecnica delle Marche, 60131 Ancona, Italy*
 # R&D Center, Automotive Cells Company (ACC), 136 quater, Avenue d'Aquitaine, 33520 Bruges, France

Experimental Section

1. Materials for the Synthesis

Dimethyl sulfoxide (DMSO), anhydrous dimethylacetamide (DMAc), dichloromethane (DCM), ethyl acetate (EtOAc), methanol (MeOH), anhydrous ethanol (EtOH), copper (Cu) powder (average particle size ~5 μm), *N*-bromosuccinimide (NBS, 99%), concentrated sulfuric acid (H_2SO_4, 96%) and anhydrous ethylene carbonate (EC, 99%) were purchased from Sigma Aldrich. Potassium carbonate (K_2CO_3, 99%) and toluene were purchased from Acros Organics. 1,1,2,2,-tetrafluoro-2-(1,1,2,2,-tetrafluoro-2-iodoethoxy)ethane sulfonyl fluoride ($ICF_2CF_2OCF_2CF_2SO_2F$) was purchased from Interchim. Anhydrous lithium hydroxide (LiOH, 98%) and anhydrous magnesium sulfate ($MgSO_4$, 97%) were supplied by Alfa Aesar and trifluoromethanesulfonamide ($CF_3SO_2NH_2$, 99%) was supplied by FluoroChem. All chemicals were used as received unless otherwise noted. Triethylamine (TEA, 99%) and acetonitrile (ACN), purchased from Sigma Aldrich, were distilled from calcium hydride (CaH_2, 98%, Acros Organics) prior to use. n-Hexane (>95%), purchased from Sigma Aldrich, was distilled in vacuo before use. 4,4'-Difluorodiphenyl sulfone (DFDPS, >98%), 4,4'-biphenol (BP, 99%), and 4,4'-dihydroxydiphenyl sulfone (DHDPS, 99%), purchased from Alfa Aesar, were recrystallized from isopropanol (Alfa Aesar) prior to use. Decafluorobiphenyl (DFBP, 99%), purchased from FluoroChem, was sublimated before use. The solvents used for the NMR spectroscopy experiments were purchased from Acros Organics ($CDCl_3$, 99.8+% D + 0.03% (v/v) TMS) and VWR (acetone-d_6, 99.8% D and DMSO-d_6, 99.8% D + 0.03% (v/v) TMS).

2. Materials for the Electrochemical Characterization

Tetra-n-butylammonium tetrafluoroborate (TnBATFB, ≥99%) and diphenyl ether (DPE, ≥99%) were purchased from Alfa Aesar, ultra-dry acetonitrile (max. 0.001% H_2O) under inert gas atmosphere was supplied by Merck, and decafluorodiphenyl ether (DFDPE, ≥95%) by Enamine. Acetonitrile was used in the glovebox as received, TnBATFB and DFDPE were dried under vacuum (~10^{-3} mbar) at elevated temperature (80 °C) at a Schlenk line prior to the transfer into the glovebox. DPE was degassed repeatedly (5x) under vacuum (~10^{-3} mbar) at a Schlenk line prior to the transfer into the glovebox.

3. Synthesis of the Perfluorosulfonimide Ionic Functions (I-psiLi)

The ionic function, *N*-(trifluoromethanesulfonyl)-1,1,2,2-tetrafluoro-2-(1,1,2,2-tetrafluoro-2-iodoethoxy)ethanesulfonamide lithium ($ICF_2CF_2OCF_2CF_2SO_2N^-(Li^+)SO_2CF_3$ or I-psiLi), was synthesized by following a procedure reported elsewhere.[1] In a typical protocol, 8.400 g (0.0563 mol) $CF_3SO_2NH_2$ were introduced into a 100-mL two-neck round bottom flask, charged with an air condenser and a magnetic stirrer. Then, 10.452 g (0.103 mol) of TEA, freshly distilled from CaH_2, and 20 mL of ACN freshly distilled from CaH_2, were added. The mixture was stirred to dissolve the solid phase and 20.000 g (0.0469 mol) of $ICF_2CF_2OCF_2CF_2SO_2F$ were added. The mixture was warmed to 40 °C and the reaction was performed at this temperature for ~36–40 h. The reaction progress was monitored by ^{19}F NMR spectroscopy. When the peak corresponding to SO_2F (44.77 ppm) disappeared, the reaction was stopped. The resulting red mixture was loaded into a rotary evaporator at 40 °C to remove the solvent. The residue was dissolved in (200–250 mL) DCM, washed with 1000 mL distilled water, and dried over anhydrous magnesium sulfate. A red oil was obtained after removing the solvent using a rotary evaporator at 40 °C.
This red oil was dissolved in 0.5M LiOH (using a 5% molar excess of LiOH). After stirring the solution for 15 min, the water was removed by freeze-drying. The resulting viscous oil was dissolved in ethyl acetate, dried over anhydrous magnesium sulfate, and the solvent was removed by rotary evaporation. The residue was dried in vacuo at 40 °C for 24 h to obtain a light-yellow solid. The final chemical yield of the I-psiLi synthesis was ~65–70%. The synthesis procedure of I-psiLi is illustrated in **Figure S1** and its ^{19}F NMR spectrum is presented in **Figure S2**.

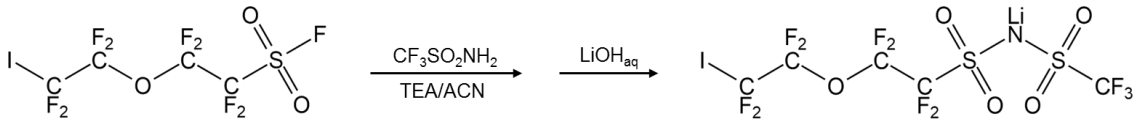

Figure S1. Synthesis procedure of I-psiLi.

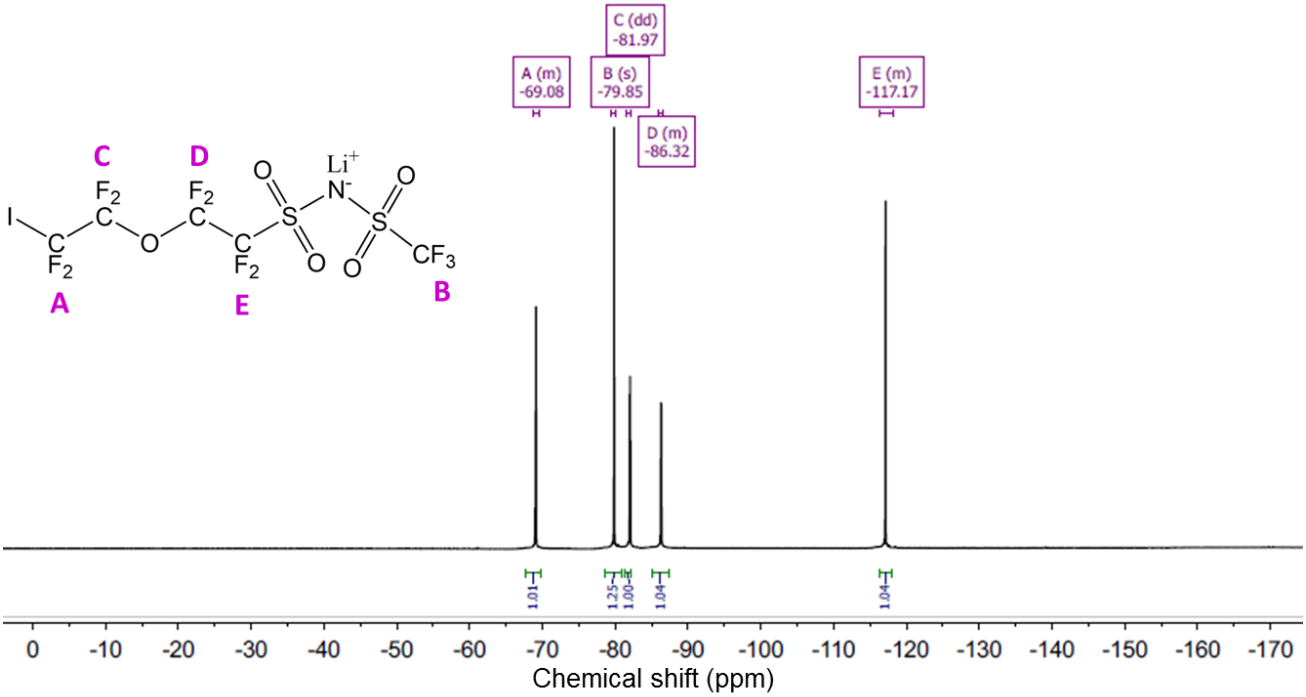

Figure S2. ^{19}F NMR spectrum of I-psiLi dissolved in $(CD_3)_2CO$.

4. Synthesis of 3,3'-Dibromo-4,4'-difluorodiphenyl sulfone (DBDFDPS)

DFDPS (12.7 g, 0.05 mol) and concentrated H_2SO_4 (96%) (65 mL) were charged at room temperature into a 100 mL three-neck round-bottom flask equipped with a mechanical stirrer, a condenser, and an argon inlet-outlet. After the solid was dissolved, NBS (19.56 g, 0.11 mol, 2.2 equiv.), divided into three portions, was added in 15 min intervals. The reaction was performed at room temperature for another 6 h under vigorous stirring. Subsequently, the reaction mixture was poured into 250 mL of ice/water mixture to precipitate the solid. Next, the solid was filtered and washed with water (300 mL), followed by n-hexane (50 mL). The final product was recrystallized twice from a 1:1 ethanol:methanol mixture to obtain 3,3'-dibromo-4,4'-difluorodiphenyl sulfone (DBDFDPS) with a yield of 60-70%. The synthesis procedure of DBDFDPS monomer is illustrated in **Figure S3** and the corresponding ^{1}H and ^{19}F NMR spectra are shown in **Figure S4**.

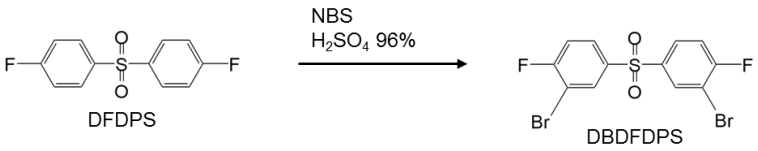

Figure S3. Synthesis procedure of the DBDFDPS monomer.

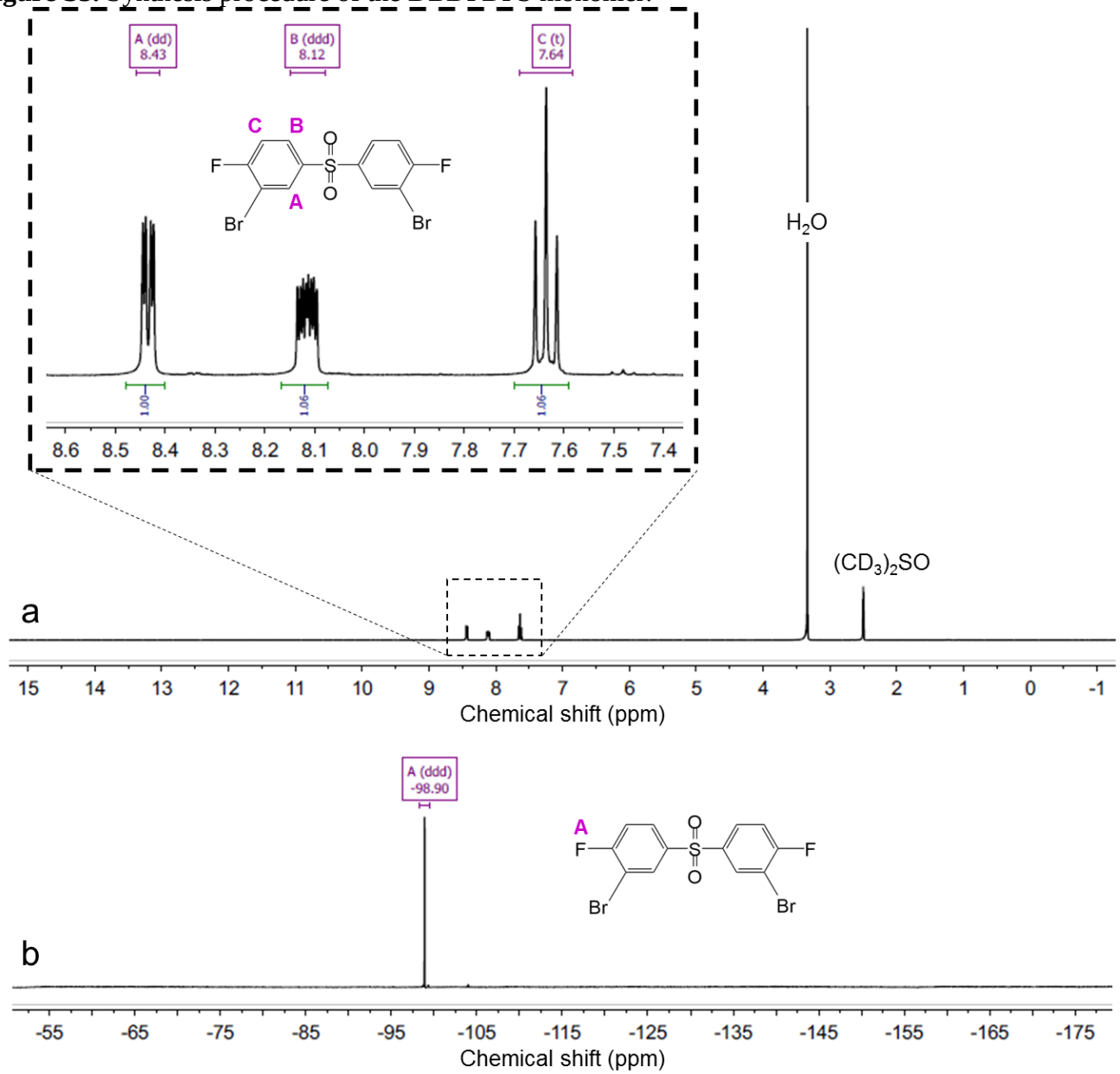

Figure S4. ^{1}H (a) and ^{19}F (b) NMR spectra of the DBDFDPS monomer dissolved in $(CD_3)_2SO$.

5. Synthesis of the PES-BPES Multi-Block Copolymer

The intermediate multi-block co-poly(arylene ether sulfone) bearing bromine groups, namely PES-BPES XY where X and Y indicate the molecular weight of the hydrophobic PES block and the brominated BPES block, respectively, in kg/mol, was obtained directly via co-polycondensation of the monomers using a one-pot-two-step synthesis.[2] For the synthesis of PES-BPES-1515, a 100 mL three-neck round bottom flask, equipped with a mechanical stirrer, a condenser, an argon inlet-outlet, and a Dean-Stark trap, was charged with DFDPS (2.0000 g, 7.866 mmol) and BP (1.5049 g, 8.082 mmol). DMAc (14 mL) was added to provide a concentration of around 25% (w/v). After the mixture was dissolved entirely, K_2CO_3 (3.35 g, 24.2 mmol) and 7 mL toluene, the azeotroping agent, were added. The ratio of DMAc to toluene (v/v) was 2:1. The reaction bath was heated to 150 °C and kept at this temperature for 4 h to dehydrate the system. Subsequently, the bath temperature was slowly raised to 160 °C to remove the toluene, followed by a decrease in temperature of the reaction bath back to 150 °C. The polymerization was allowed to proceed at this temperature for 24 h. Then, the reaction bath was cooled down to 60 °C, K_2CO_3 (3.25 g, 23.5 mmol) was introduced, and the solution containing 3.3199 g of DBDFDPS (8.057 mmol) and 1.4602 g BP (7.842 mmol) in 20 mL of DMAc (≈ 25 % m/v) was added dropwise. After that, 17 mL toluene were added, and the temperature was again increased to 150 °C for 4 h to dehydrate the system, followed by the controlled removal of toluene at 160 °C, and the polymerization at 150 °C for another 24 h. Finally, the reaction mixture was precipitated into 1000 mL distilled water and rinsed with distilled water until a neutral pH was reached, followed by a washing step with methanol. The final product was dried in vacuo at 80 °C for 24 h. The synthesis procedure of the PES-BPES block copolymer is illustrated in **Figure S5** and its ^{1}H NMR spectrum is presented in **Figure S6**.

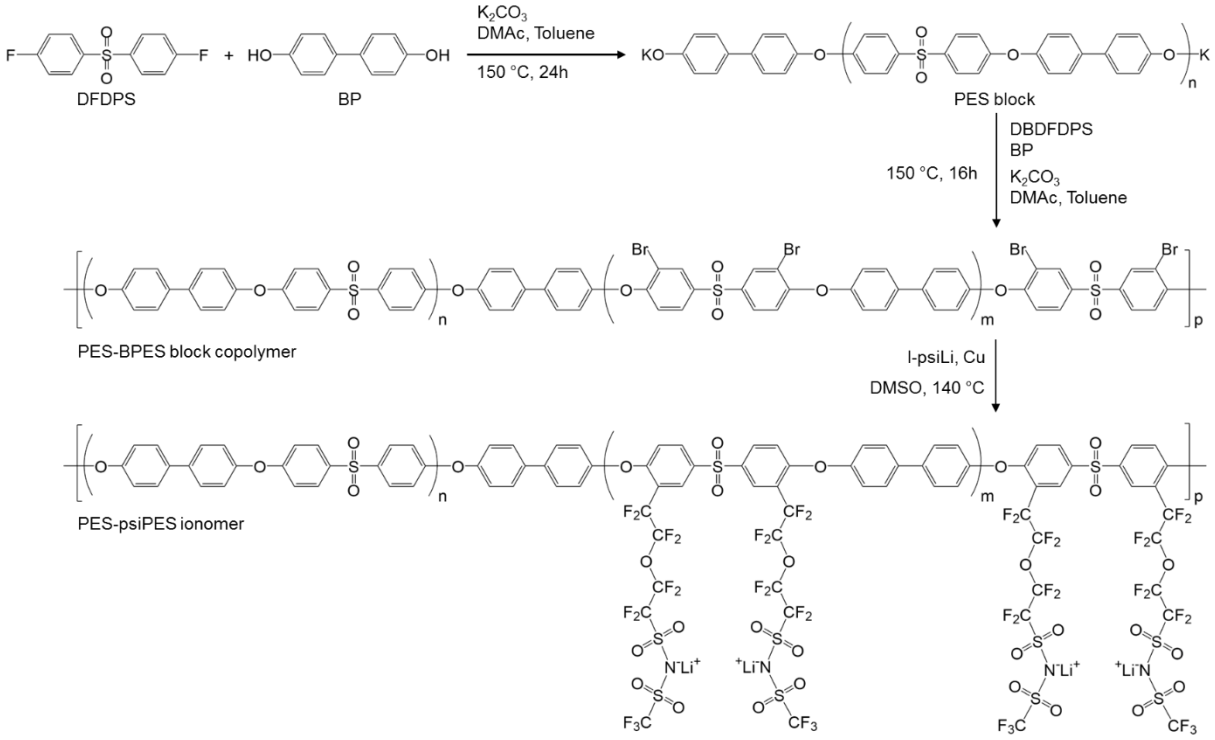

Figure S5. Synthesis procedure of the PES-BPES multi-block copolymer and PES-psiPES ionomer.

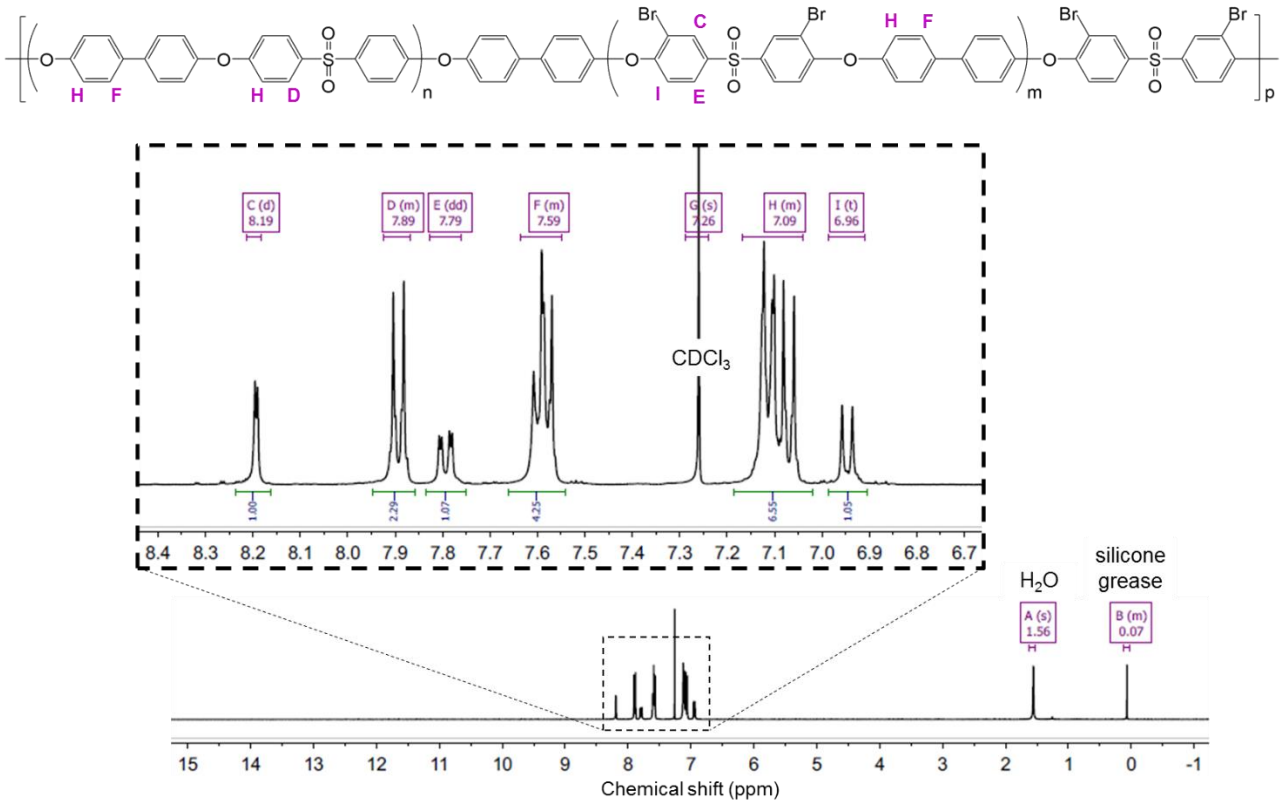

Figure S6. ^{1}H NMR spectrum of the PES-BPES multi-block copolymer dissolved in $CDCl_3$.

6. Synthesis of the PES-psiPES Multi-Block Copolymer via Post-Polymerization Modification

The ionic function (I-psiLi) was coupled with the PES-BPES copolymer via a copper-catalyzed Ullmann coupling reaction. For the synthesis of PES-psiPES-1515, a 100-mL three-neck round bottom flask (equipped with a mechanical stirrer, a condenser, and an argon inlet-outlet) was charged with PES-BPES (4.000 g, 8.42 mmol of Br), 40 mL DMSO, and 10 mL toluene. Toluene was used to prevent the precipitation of PES-BPES owing to the solvent competition when I-psiLi was introduced. When the polymer was fully dissolved at 60 °C under stirring, copper powder (2.675 g, 42.09 mmol, 5 equiv. to Br) was added and the bath temperature was set at 120 °C for 2 h. Then, the reaction temperature was increased to 140 °C and I-psiLi (7.086 g, 12.63 mmol, 1.5 equiv. to Br) dissolved in 15 mL DMSO was slowly added drop-by-drop in 1 h to avoid the precipitation of the PES-BPES copolymer. The reaction was performed at that temperature for 24 h under vigorous stirring. Subsequently, the cooled reaction mixture was precipitated into 1000 mL of a 1M HCl solution and kept under vigorous stirring for 24 h. The obtained ionomer was further purified by dissolving it in 100 mL DMSO, followed by centrifugation at 5000 rpm for 15 min to remove the solid impurities, precipitating the homogenous solution into 1000 mL of 1M HCl solution, and stirring the solution until the ionomer particles became transparent. The purified ionomer was washed several times with distilled water until a neutral pH was obtained. The ionomer in its acidic form was deprotonated with a 0.5M LiOH solution to obtain the ionomer in its lithiated form, followed by washing several times with distilled water until a neutral pH was reached. The ionomer particles were filtered and dried in vacuo at 100 °C for 24 h before use. The synthesis procedure of the PES-psiPES ionomer is illustrated in **Figure S5**. The ^{1}H and ^{19}F NMR spectra of PES-psiPES ionomer are presented in **Figure S7**.

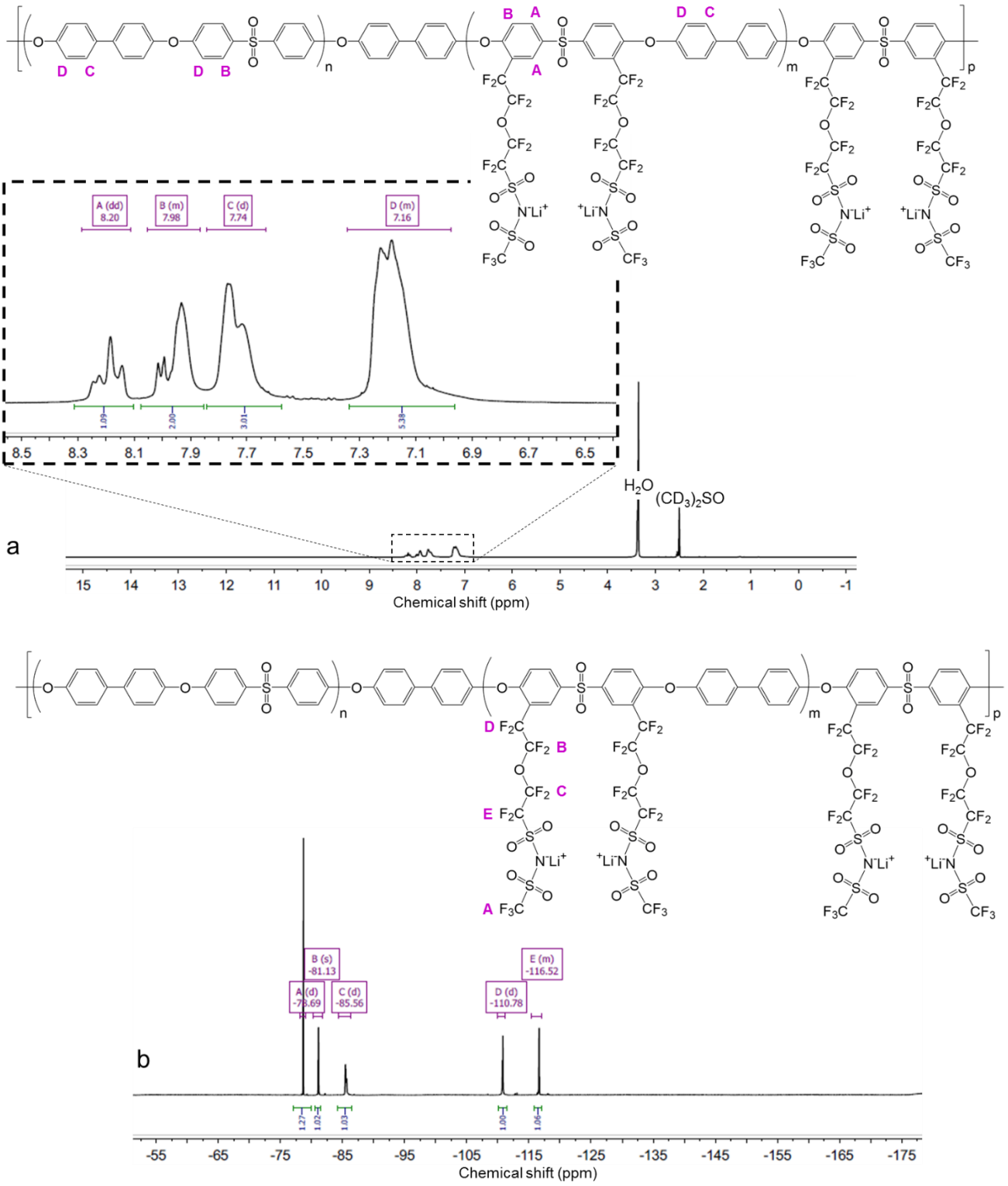

Figure S7. ^{1}H (a) and ^{19}F (b) NMR spectra of the PES-psiPES ionomer dissolved in $(CD_3)_2SO$.

7. Preparation of the Ionomer Films

The ionomer films (with a thickness of around 50 μm) were obtained by casting from DMSO, followed by thermal annealing as reported elsewhere.[1,3] Generally, 1.00 g of the ionomer in its lithiated form was introduced into 14 mL of DMSO, followed by stirring the mixture at 60 °C for 24 h to obtain a homogeneous solution. Subsequently, the polymer solution was centrifuged at 5000 rpm for 15 min to remove solid impurities and left in vacuo to remove gas bubbles for 15 min. The homogeneous mixture was cast onto a clean glass substrate using an Elcometer 4340 Automatic Film Applicator. The solvent was evaporated at 60 °C in an oven for 48 h to obtain the ionomer membranes, which were subjected to an additional thermal treatment at 150 °C for 24 h in a closed vacuum chamber. The annealed membranes were immersed in distilled water for 48 h and washed several times with water to completely remove residual traces of the casting solvent.

8. Preparation of Polymer Electrolyte Membranes

The electrolyte membranes were obtained via doping the dried ionomer films with different amounts of EC, as reported elsewhere.[1] The solvent content (*SC*, wt.%), controlled by the immersing time, was calculated according to **Equation 1**:

$$SC = \frac{W_s - W_d}{W_s} \times 100\% \quad (\mathbf{1})$$

where W_s and W_d are the weight of the swollen and dried membranes, respectively.

The Li^+ ion concentration (C_{Li}, mol of Li^+ ions per kg of electrolyte) in the dried ionomer films was obtained from the IEC of the dry membranes. The lithium concentration in the solvent-doped membranes was calculated by **Equation 2**:

$$C_{Li} = \frac{IEC}{1 + 0.01 \times SU} \quad (\mathbf{2})$$

where *SU* (%) is the solvent uptake of the dry ionomer membrane, as calculated by **Equation 3**:

$$SU = \frac{W_s - W_d}{W_d} \times 100\% \quad (\mathbf{3})$$

where W_s and W_d are the weights of the swollen and dry membranes, respectively.

9. Characterization

NMR Spectroscopy. The chemical structure of the monomers and block copolymers was confirmed by NMR spectroscopy using a Bruker Ascend™ 400 apparatus at 25 °C. Samples were dissolved in deuterated solvents and injected into NMR tubes.

Ion-Exchange Capacity (IEC). The IEC (meq. Li^+/g) of the ionomer was determined via acid-base titration of the acidified membranes.

Thermal Properties. The glass transition temperature (T_g) of the samples was determined using a differential scanning calorimeter (1 STAR^e DSC System from Mettler-Toledo). Around 10 mg of sample were sealed in an aluminum capsule inside the glovebox. The measurements were carried out at a heating rate of 10 °C min^{-1} from 25 to 325 °C for the dry ionomer film and from -150 to 250 °C for the EC-comprising membranes under an argon flux of 50 mL min^{-1}. The thermal stability of the ionomer was analyzed from 50 to 750 °C with a heating rate of 10 °C min^{-1} using a thermogravimetric analyzer (1 STAR^e TGA System from Mettler-Toledo) under synthetic air (80% N_2 and 20% O_2) with a flow rate of 20 mL min^{-1}.

Size Exclusion/Gel Permeation Chromatography (SEC/GPC): The molecular weight of the polymer samples was determined by gel permeation chromatography (GPC) using a multi-detector Malvern Panalytical OmniSEC Resolve/Reveal system equipped with a three-column setup (Viscotek D5000-D3000-D2000). The eluent was a 0.05M LiBr solution in *N*,*N*-dimethylformamide (DMF) with a flux rate of 0.8 mL min^{-1}. The sample analysis was performed using a refractive index (RI) detector, accompanied by a UV detector, detectors for low-angle and right-angle light scattering (LALS and RALS), as well as a viscometer. The molecular weight was derived from the refractive index and light scattering, utilizing a universal calibration method with one narrow poly(methyl methacrylate) (PMMA) standard, which was subsequently verified by analyzing an additional broad PMMA standard. To prepare the GPC samples, 20-25 mg (weighed precisely) of each polymer sample were dissolved in 10 mL of the eluent, followed by filtration through a syringe filter. Two injections per sample with an injection volume of 100 µL each were carried out to ensure data consistency. The OmniSEC software was used to analyze the data obtained.

Table S1: Molecular weights of the SIC-BCE with the (**1**) fluorinated and (**2**) non-fluorinated backbone determined by gel permeation chromatography (GPC).

	M_n [kg mol^{-1}]	M_w [kg mol^{-1}]	PDI
1	264	724	2.7
2	260	590	2.3

Ionic Conductivity: Symmetric Cu‖Cu cells were used to determine the ionic conductivity at different temperatures. Therefore, the polymer membranes dopped with the desired EC content were sandwiched between two copper foils (35 µm thick) in pouch cells in a dry room. After sealing the pouch cells using a vacuum sealer (Audiovac VMS 163, Audion), the cells were stored at 40 °C for at least 24 h prior to the measurements. Electrochemical impedance spectroscopy (EIS) was conducted by means of a Solartron SI 1260/1287 Impedance Analyser (frequency range: 1 Hz to 1 MHz) at different temperatures in a Binder climatic chamber KB23 with 3 h resting time after a temperature change prior to the next measurement. The subsequent analysis of the data was performed with the RelaxIS 3 software (rhd instruments) using an *RP* fitting model. The ionic conductivity (σ) was determined by referring to the thickness d of the polymer membrane (after the measurement, determined with Mitutoyo Absolute digital thickness gauge 547-401) and the area A of the polymer membrane covered by both copper electrodes using the following equation:

$$\sigma = \frac{d}{RA}$$

Lithium Stripping/Plating: Lithium stripping/plating experiments were performed in coin cells (CR2032, Hohsen) at 40 °C (Binder climatic chamber KB 115), using a Maccor 4000 battery testing system. Disk-shaped lithium foils (14 mm in diameter, 500 µm thickness, battery grade, Honjo) were placed on stainless steel spacers (16 mm, 0.5 mm thickness), followed by sandwiching the EC-doped polymer membranes between the lithium disks in an argon-filled glovebox (MBRAUN MB-200-MOD, H_2O/O_2 <1 ppm). The coin cells were sealed using a hydraulic coin cell crimping machine (MSK-110, MTI Corp, pressure of ~800 psi). The current density was varied, i.e., 5, 10, 20, 50, 100, and 200 mA cm^{-2}, and the current was reversed after 1 h intermitted by a 5 min rest step.

Electrochemical Stability Window (ESW) of the Polymer Membranes: For the determination of the electrochemical stability via linear sweep voltammetry (LSV), two-electrode pouch cells with nickel foil as the working electrode and lithium foil (50 µm thickness, battery grade, Honjo) as the counter electrode were assembled in a dry room. The measurements were conducted using a BioLogic VMP3 Multichannel Potentiostat at a temperature of 20 °C (Binder climatic chamber KB23) and a sweep rate of 1 mV s^{-1} after a rest time of at least 24 h. The cut-off voltages were set to -2.0 V and +6.0 V. Fresh cells were used for each LSV experiment.

ESW of the Model Compounds: LSV was also employed to determine the electrochemical stability of model compounds in Swagelok-type T-cells, including a platinum disk as working electrode (eDAQ ET075-1, carefully polished before use, following the procedure recommended by eDAQ) and activated carbon (the preparation is described elsewhere[4]) as counter and reference electrodes (11 mm and 8 mm in diameter, respectively). Glass fiber separators (Whatman GF/A) were used to separate the electrodes from each other. The liquid electrolyte (0.1M TnBATFB in acetonitrile), either pure or containing the dissolved model compound DPE or DFDPE, was dropped on the glass fiber separator (200 µL for 12 mm separator,

100 µL for 10 mm separator) and the cell was subsequently closed. Measurements were conducted using a BioLogic VMP 3 potentiostat at 20 °C (Binder KB 115 climatic chamber) and a sweep rate of 1 mV s^{-1} with a lower and upper cutoff voltage of -4 V and +4 V, respectively. According to the literature, the potential of the activated carbon quasi-reference electrode (AC QRE) vs. Li^+/Li was set to +3 V.[5]

Small-Angle X-ray Scattering (SAXS): SAXS patterns were collected using a Xeuss 3.0c (Xenocs – Grenoble, France) equipped with an Eiger2 1M detector. The sample-to-detector distance was set to 1100 mm, obtaining an overall usable Q-range from 0.00014 to 0.247 $Å^{-1}$. A Cu K_α source was used with a beam size of 0.35x0.35 mm^2, obtaining a flux of ~10^5 photons per second. The samples were stuck to a perforated metal plate using standard scotch tape. Powders were simply stuck to the tape, completely covering the holes of the plate, while membranes were stuck in a way that only the membrane was covering the hole. The sample chamber of the instrument was kept under vacuum (p = 250 µbar) during the experiment. Each measurement was performed for 30 min to ensure a good signal-to-noise ratio. The collected 2D scattering patterns were azimuthally integrated over the entire circumference to obtain the scattering curves as a function of Q. The intensity was scaled to absolute units using the sample transmission and the calibration with a glassy carbon secondary standard. When needed, the plain scotch tape background was also collected and subtracted from the total scattering curve. Data treatment was performed with the Xsact software from Xenocs.

X-ray Photoelectron Spectroscopy (XPS). The sample preparation was carried out in an argon-filled glovebox (MBRAUN MB-200-MOD, H_2O/O_2 <1 ppm) by immersing a stripe of lithium metal (500 µm thickness, battery grade, Honjo) in a glass vial containing either DPE or DFDPE dissolved in DPE or in an empty glass vial for the pristine lithium metal as a control sample. After 24 h, the stripes were removed from the glass vials, and any remaining traces of liquid were carefully removed. Small pieces were cut from the lithium metal stripes and stuck on carbon tape on the XPS sample holder. To avoid contact with air or moisture, the samples were transferred to the load lock of the XPS. The chemical state of the sample surfaces was analyzed by XPS using a Specs XPS system with a Phoibos 150 energy analyzer. The spectra were recorded using monochromatized Al K_α radiation (400 W, 15 kV) at a detection angle of 45° with pass energies of 90 eV and 30 eV for the survey and detail measurements, respectively. Sample charging was relatively small; all binding energies were calibrated to the C1s peak of adventitious carbon at 284.8 eV. The peak fit of the XPS results was done with CasaXPS, using Shirley-type backgrounds and Gaussian-Lorentzian peak shapes.

Simulation of the Model Compounds: DFT calculations were performed with Gaussian16[6] at the B3LYP/6-311++G** level of theory. The starting guess geometries were hand-drawn using Avogadro[7] and then optimized using ultrafine thresholds. The Gibbs free energies were obtained by performing a frequency calculation on the obtained configurations, including the thermal (298 K) and zero-point-energy contributions. No imaginary frequency was observed for the optimization step, confirming the obtained geometry as a minimum of the potential energy surface. The effect of the solvation shell was included by means of a Polarizable Continuum Model (PCM) using the static and dynamic dielectric constant of acetonitrile as implemented in Gaussian16. A different set of dielectric constants was used to check the stability in the polymer, where EC was used as filler. For this, the static and dynamic dielectric constants of pure EC (95.3 and 2.005) were used. The geometries obtained from the optimization of the singlet states (i.e., the neutral ethers) were then used as starting configurations for the two doublet states, where a single electron was either injected (reduction) or removed (oxidation) from the system. The energy values of the doublet states were obtained by single point calculations because the electron exchange is much faster than the nuclear re-arrangement. The molecules were then allowed to relax reaching a new minimum of the potential energy surface. The newly adopted geometry can provide hints on the decomposition pathways. The Nernst-Einstein relationship then returned the absolute redox potentials, which

were converted in potentials vs. Li^+/Li by adding and subtracting 1.38 ±0.2 V (considering 4.6 ±0.2 V for the standard hydrogen electrode[8,9] and -3.04 V for the Li^+/Li redox couple) for the reduction and oxidation, respectively. A complete overview on the methodology can be found elsewhere.[10,11] In summary, the following equations were used:

$$\Delta G_{298}^{RedOx} = G_{298}^{Ox} - G_{298}^{Red} \quad (1)$$

$$V_{Abs} = \frac{\Delta G_{298}^{RedOx}}{n \cdot F} \quad (2)$$

$$V_{vs.Li} = V_{Abs} + \left(V_{Abs}^{SHE} + V_{Li^+/Li}\right) \quad (3)$$

where ΔG_{298}^{RedOx} is the reduction free energy difference at 298 K; G_{298}^{Ox} and G_{298}^{Red} are the Gibbs free energy of the oxidized and reduced states, respectively; V_{Abs} is the absolute reduction potential; *n* is the number of exchanged electrons; *F* is the Faraday constant; $V_{Li^+/Li}$ is the standard reduction potential of the Li^+/Li redox couple; V_{Abs}^{SHE} is the absolute potential of the standard hydrogen electrode; and $V_{vs.Li}$ is the reduction potential vs. the Li^+/Li redox couple. All the energy terms are expressed in kJ mol^{-1}, the potentials values are provided in V, and the Faraday constant is 96.485 kC mol^{-1}.

Table S2: Gibbs energy values obtained from the calculations and the results of the application of Equations 1-3 for both diphenyl ether and decafluorodiphenyl ether in acetonitrile and ethylene carbonate, respectively.

	Diphenyl ether *(in acetonitrile)*	**Decafluorodiphenyl ether** *(in acetonitrile)*	**Diphenyl ether** *(in ethylene carbonate)*	**Decafluorodiphenyl ether** *(in ethylene carbonate)*
$G_{298}^{Singlet}$ *[Hartree]*	-538.512	-1531.193	-538.509	-1531.193
G_{298}^{Red} *[Hartree]*	-538.564	-1531.270	-538.560	-1531.271
G_{298}^{Ox} *[Hartree]*	-538.278	-1530.923	-538.273	-1530.925
ΔG_{298}^{Red} *[Hartree]*	0.052	0.077	0.050	0.078
ΔG_{298}^{Ox} *[Hartree]*	0.234	0.270	0.237	0.268
ΔG_{298}^{Red} *[kJ mol^{-1}]*	137.3	201.6	131.7	204.4
ΔG_{298}^{Ox} *[kJ mol^{-1}]*	615.1	708.4	621.3	704.4

V_{Abs}^{Red} *[V]*	-1.4	-2.1	-1.4	-2.1
V_{Abs}^{Ox} *[V]*	6.4	7.3	6.4	7.3
$V_{vs.Li}^{Red}$ *[V]*	0.1	-0.5	0.2	-0.6
$V_{vs.Li}^{Ox}$ *[V]*	4.8	5.8	4.9	5.7

10. Explanation on the Reallocation of the Side Chain with respect to the Polymer Backbone

The lithium moieties bearing side chains were attached to the diphenyl sulfone repeating unit in the fluorine-free polymer backbone, different from the fluorinated polymer backbone reported earlier,[1] for which the ionic side chains were attached to the biphenyl repeating unit. For comparison, both chemical structures are displayed in **Figure S8**. This difference originates from synthetical demands, since the realization of the fluorine-free polymer backbone was only possible by monomer modification prior to the polymerization reaction. In fact, the initial attempts focused on the dibromination of the 4,4'-biphenol monomer and subsequent polymerization to keep the polymer structure as consistent as possible. However, due to the high reactivity of this monomer, it turned out to be impossible to stop the reaction at the stage of dibromination only, also yielding tri- and tetrabrominated monomers as side products. While purification methods such as column chromatography, recrystallization, and sublimation allowed to reduce the amount of side products at the expense of substantially reduced yields due to the chemical similarity of the compounds, the authors were not able to receive a pure 3,3'-dibromo-4,4'-biphenol monomer. Attempts to polymerize the 3,3'-dibromo-4,4'-biphenol slightly contaminated with the tribrominated derivate failed, most likely due to the chain termination effect of having two bulky bromine atoms next to the reactive site. To illustrate this issue, an exemplary NMR spectrum of the bromination reaction of 4,4'-biphenol is shown in **Figure S9**. For this reason, the authors finally switched to the bromination of the 4,4'-difluorodiphenyl sulfone monomer since this reaction is unlikely to proceed further after having already added two atoms of bromine to the monomer due to the electron-withdrawing/deactivating effect of the fluorine substituents. The increased spacing between the two side chains attached to the diphenyl sulfone unit might potentially influence the conductivity of the polymer membranes. However, the authors did not observe any evidence for an inferior charge transport.

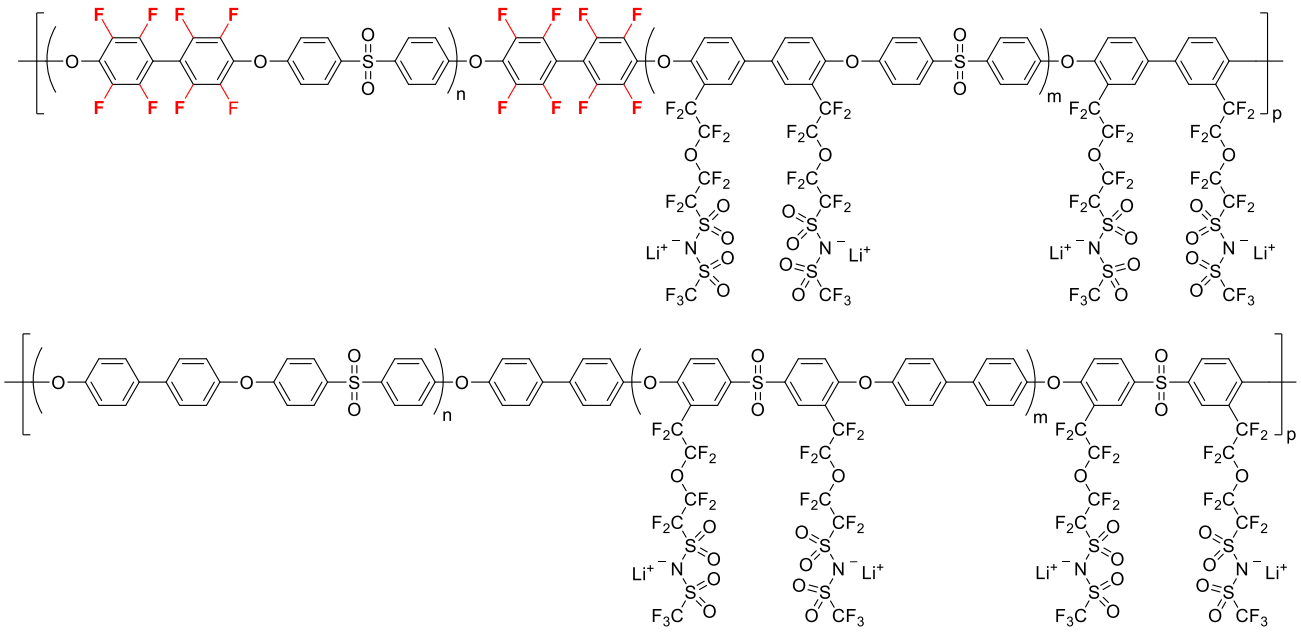

Figure S8. Chemical structures of the SIC-BCEs comprising a partially fluorinated backbone (highlighted with red color) and its fluorine-free analogue.

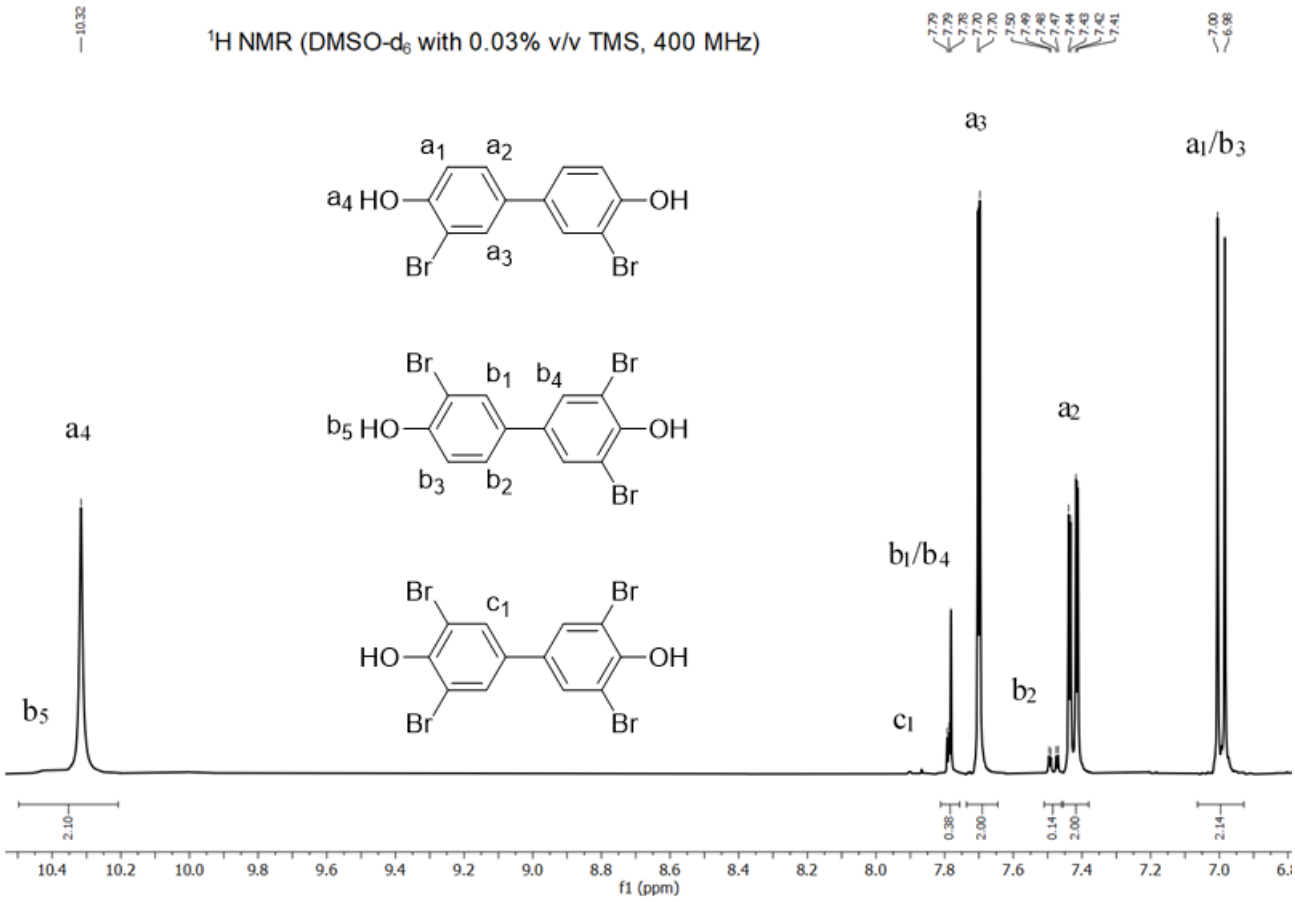

Figure S9. NMR spectrum of the product resulting from the bromination of 4,4'-biphenol, showing the dibrominated monomer as the main product, accompanied by side products originating from tri- and tetrabrominated monomers.

References

(1) Nguyen, H. D.; Kim, G. T.; Shi, J.; Paillard, E.; Judeinstein, P.; Lyonnard, S.; Bresser, D.; Iojoiu, C. Nanostructured Multi-Block Copolymer Single-Ion Conductors for Safer High-Performance Lithium Batteries. *Energy Environ. Sci.* **2018**, *11* (11), 3298–3309.

(2) Assumma, L.; Iojoiu, C.; Mercier, R.; Lyonnard, S.; Nguyen, H. D.; Planes, E. Synthesis of Partially Fluorinated Poly(Arylene Ether Sulfone) Multiblock Copolymers Bearing Perfluorosulfonic Functions. *J. Polym. Sci. Part A Polym. Chem.* **2015**, *53* (16), 1941–1956.

(3) Assumma, L.; Nguyen, H. D.; Iojoiu, C.; Lyonnard, S.; Mercier, R.; Espuche, E. Effects of Block Length and Membrane Processing Conditions on the Morphology and Properties of Perfluorosulfonated Poly(Arylene Ether Sulfone) Multiblock Copolymer Membranes for PEMFC. *ACS Appl. Mater. Interfaces* **2015**, *7* (25), 13808–13820.

(4) Barbieri, O.; Hahn, M.; Herzog, A.; Kötz, R. Capacitance Limits of High Surface Area Activated Carbons for Double Layer Capacitors. *Carbon* **2005**, *43* (6), 1303–1310.

(5) Ruch, P. W.; Cericola, D.; Hahn, M.; Kötz, R.; Wokaun, A. On the Use of Activated Carbon as a Quasi-Reference Electrode in Non-Aqueous Electrolyte Solutions. *J. Electroanal. Chem.* **2009**, *636* (1–2), 128–131.

(6) Frisch, M. J.; Trucks, G. W.; Schlegel, H. B.; Scuseria, G. E.; Robb, M. A.; Cheeseman, J. R.; Scalmani, G.; Barone, V.; Petersson, G. A.; Nakatsuji, H.; Li, X.; Caricato, M.; Marenich, A.; Bloino, J.; Janesko, B. G.; Gomperts, R.; Mennucci, B.; Hratchian, H. P.; Ort, J. V.; Fox, D. J., 2009.

(7) Hanwell, M. D.; Curtis, D. E.; Lonie, D. C.; Vandermeersch, T.; Zurek, E.; Hutchison, G. R. Avogadro: An Advanced Semantic Chemical Editor, Visualization, and Analysis Platform. *J. Cheminform.* **2012**, *4* (1), 17.

(8) Ramette, R. W. Outmoded Terminology: The Normal Hydrogen Electrode. *J. Chem. Educ.* **1987**, *64* (10), 885.

(9) Trasatti, S. The Absolute Electrode Potential: An Explanatory Note (Recommendations 1986). *Pure Appl. Chem.* **1986**, *58* (7), 955–966.

(10) Davis, A. P.; Fry, A. J. Experimental and Computed Absolute Redox Potentials of Polycyclic Aromatic Hydrocarbons Are Highly Linearly Correlated over a Wide Range of Structures and Potentials. *J. Phys. Chem. A* **2010**, *114* (46), 12299–12304.

(11) Méndez-Hernández, D. D.; Tarakeshwar, P.; Gust, D.; Moore, T. A.; Moore, A. L.; Mujica, V. Simple and Accurate Correlation of Experimental Redox Potentials and DFT-Calculated HOMO/LUMO Energies of Polycyclic Aromatic Hydrocarbons. *J. Mol. Model.* **2013**, *19* (7), 2845–2848.